

CaMKII δ , δ B or δ C, plays an important role in apoptosis of cardiomyocytes, we transfected constitutively active forms of CaMKII δ (caCaMKII δ) into cardiomyocytes. Only caCaMKII δ C, not caCaMKII δ B, increased protein levels of p53 (Figure VIB in the online-only Data Supplement). Furthermore, p53 protein levels in caCaMKII δ C-transfected cardiomyocytes did not increase with MG132 treatment compared with MOCK-treated cardiomyocytes (Figure VIC in the online-only Data Supplement). These results suggest that activation of CaMKII δ C increases apoptotic cardiomyocytes at least in part via stabilization of p53 in the DCM mouse model.

Discussion

In the present study, we established a novel mouse model of DCM to clarify the mechanisms of how mutant genes lead to DCM (Table II in the online-only Data Supplement and Figure 1). The mice expressing cardiac α -actin R312H mutant in the heart, which has been reported to cause DCM in humans,⁵ showed dilatation and dysfunction of left ventricle with an increase in ANP messenger RNA levels, which is consistent with human heart failure (Figure 1A and 1E and Table II and Figure III in the online-only Data Supplement). Higher heart rate and hyperphosphorylated phospholamban (Ser16) (Table II in the online-only Data Supplement and Figure 5A) suggest the activation of the sympathetic nervous system to compensate for reduced cardiac systolic function, resulting in an increase in spontaneous Ca²⁺ sparks and Ca²⁺ waves (Table III in the online-only Data Supplement). Myofilament Ca²⁺ sensitivity was decreased in mActin-Tg mice even at 2 months of age (Figure 4B), when cardiac phenotypes such as left ventricular dilatation and cardiac fibrosis were not recognized (Table II in the online-only Data Supplement and Figure 1). These results suggest that the decrease in myofilament Ca²⁺ sensitivity is a primary cause of, not a secondary result from, cardiac dysfunction. Because these phenotypes were quite similar to those of human DCM, mActin-Tg mice are useful for examining the underlying mechanisms of how gene mutations lead to DCM.

There was no significant difference in the peak amplitude of Ca²⁺ transients between wild-type littermates and mActin-Tg mice (Figure IVC in the online-only Data Supplement), suggesting that global Ca²⁺ levels underlying each contractile cycle do not differ between the 2 groups. It has been reported that the peak amplitude of Ca²⁺ transients, which is associated with decreased Ca²⁺ sensitivity and systolic dysfunction, is higher in another mouse model of DCM,⁷ suggesting that Ca²⁺ transients are augmented to compensate for decreased myofilament Ca²⁺ sensitivity in this model. In mActin-Tg mice, despite the preserved Ca²⁺ transients (Figure IVC in the online-only Data Supplement), global cardiac function was gradually impaired (Table II in the online-only Data Supplement). Local Ca²⁺ concentration has been reported to be important for the activation of Ca²⁺-dependent enzymes such as calcineurin, calpain, and CaMKII in cardiomyocytes.³⁰ The activation of these molecules in mActin-Tg mice (Figures 4D, 4E, and 5A) might be attributed to an increase in local Ca²⁺ levels. It still remains to be determined whether local Ca²⁺ levels are really in-

creased and, if so, how the decrease in Ca²⁺ sensitivity increases local Ca²⁺ levels.

Recent reports have shown that CaMKII δ plays a crucial role in cardiovascular diseases.^{16,31} The transgenic mice that overexpressed CaMKII δ showed heart failure with systolic dysfunction and left ventricular dilatation.^{25,26} In this study, CaMKII δ was activated in the hearts of mActin-Tg mice (Figure 5A), and inhibition of CaMKII δ by KN-93 or AC3-I ameliorated cardiac dysfunction in mActin-Tg mice (Figure 5C and 5D), suggesting that CaMKII δ also plays an important role in gene mutation-induced cardiac dysfunction.

It has been reported that apoptosis of cardiomyocytes is observed in hearts of human DCM¹⁰ and that cardiomyocyte death could cause cardiac dysfunction.²⁰ However, it remains unclear whether apoptosis of cardiomyocytes causes cardiac dysfunction and how cardiomyocyte apoptosis is induced in hearts of DCM. In this study, there were more apoptotic cardiomyocytes in mActin-Tg mice (Figure 2A), and cardiac function was improved by protecting cardiomyocytes from apoptosis through overexpression of Bcl-2 (Figure 2B). These results suggest that cardiomyocyte apoptosis plays a crucial role in the development of DCM. Several key proapoptotic and antiapoptotic genes have been reported to be positively or negatively regulated by p53, and increased expression of p53 induces left ventricular dilatation and dysfunction in mice deficient in MDM4, an E3 ligase for p53.²³ Furthermore, we have recently demonstrated that p53 is critically involved in pressure overload-induced cardiac dysfunction.²² The protein levels of p53 were increased in mActin-Tg mice (Figure 3A), and loss of a single p53 allele reduced the number of apoptotic cardiomyocytes (Figure 3D) and improved cardiac function (Figure 3B). These results suggest that p53 is critically involved in induction of cardiomyocyte apoptosis, resulting in left ventricular dysfunction in the mouse model of DCM.

The present study indicates that p53 might be a therapeutic target for DCM. In this study, CaMKII δ was activated in the hearts of mActin-Tg mice (Figure 5A), and the inhibition of CaMKII δ attenuated the increase in p53 protein levels (Figure 6A and Figure VIA in the online-only Data Supplement), suggesting that CaMKII δ regulates protein levels of p53 in the DCM model mice. Although it remains to be determined how CaMKII δ regulates protein levels of p53, inhibition of CaMKII δ may become a new therapeutic strategy for DCM patients by reducing p53 protein levels in the heart.

Limitations

This study has a couple limitations. First, we cannot completely rule out the nonspecific effects of overexpression of cardiac α -actin gene with tag because of a lack of transgenic mice that overexpress wild-type cardiac α -actin gene. However, we think the cardiac dysfunction observed in mActin-Tg was due to cardiac expressions of the cardiac α -actin R312H mutant in the heart, not to high-level expressions of the cardiac α -actin protein with tag because of the following reasons: We obtained 3 independent founders of the transgenic mice, and the reduction in cardiac function was well correlated with protein levels of the cardiac α -actin R312H mutant (Figure I in the online-only Data Supplement). An-

other transgenic mouse that expressed cardiac α -actin A331P mutant with an HA tag in the heart did not show cardiac dysfunction (Table I in the online-only Data Supplement), although the protein levels of the mutant in the A331P mutant transgenic mice were almost same as those of the R312H mutant in line 307, which had the highest expression (Figure II in the online-only Data Supplement). Second, we found that CaMKII δ C increases p53 protein levels mainly by its stabilization, but the underlying mechanisms remain to be determined.

Acknowledgments

We thank J. Robbins (Children's Hospital Research Foundation, Cincinnati, Ohio) for a fragment of α -myosin heavy chain gene promoter, J.D. Molkentin (Children's Hospital Research Foundation, Cincinnati, Ohio) for NFAT-luciferase reporter transgenic mice, M.D. Schneider (Imperial College, London, UK) for Bcl-2 transgenic mice, and E.N. Olson (UT Southwestern Medical Center, Dallas, Tex) for constitutively active forms of CaMKII δ . We thank E. Fujita, R. Kobayashi, Y. Ishiyama, M. Ikeda, I. Sakamoto, A. Furuyama, and Y. Ohtsuki for technical support, as well as M. Iiyama, K. Matsumoto, Y. Ishikawa, and Y. Yasukawa for animal care.

Sources of Funding

This work was supported by a Grant-in-Aid for Scientific Research on Priority Areas (to Dr Komuro) and a Grant-in-Aid for Scientific Research (C) (20590857 to Dr Oka) from the Ministry of Education, Culture, Sports, Science and Technology; the Japan Heart Foundation/Novartis Grant for Research Award on Molecular and Cellular Cardiology; Japan Foundation for Applied Enzymology; Suzuken Memorial Foundation; and Mitsubishi Pharma Research Foundation (to Dr Toko). This work was supported by National Institutes of Health grants R01 HL079031, R01 HL070250, and R01 HL096652 and by the Fondation Leducq Award to the Alliance for Calmodulin Kinase Signaling in Heart Disease (to Dr Anderson).

Disclosures

Dr Anderson is named on patents claiming to treat heart failure by CaMKII inhibition and is a cofounder of Allosteros. The other authors report no conflicts.

References

- Michels VV, Moll PP, Miller FA, Tajik AJ, Chu JS, Driscoll DJ, Burnett JC, Rodeheffer RJ, Chesebrough JH, Tazelaar HD. The frequency of familial dilated cardiomyopathy in a series of patients with idiopathic dilated cardiomyopathy. *N Engl J Med*. 1992;326:77–82.
- Maron BJ, Towbin JA, Thiene G, Antzelevitch C, Corrado D, Arnett D, Moss AJ, Seidman CE, Young JB. Contemporary definitions and classification of the cardiomyopathies: an American Heart Association scientific statement from the Council on Clinical Cardiology, Heart Failure and Transplantation Committee; Quality of Care and Outcomes Research and Functional Genomics and Translational Biology Interdisciplinary Working Groups; and Council on Epidemiology and Prevention. *Circulation*. 2006;113:1807–1816.
- Ahmad F, Seidman JG, Seidman CE. The genetic basis for cardiac remodeling. *Annu Rev Genomics Hum Genet*. 2005;6:185–216.
- Knoll R, Hoshijima M, Hoffman HM, Person V, Lorenzen-Schmidt I, Bang ML, Hayashi T, Shiga N, Yasukawa H, Schaper W, McKenna W, Yokoyama M, Schork NJ, Omens JH, McCulloch AD, Kimura A, Gregorio CC, Poller W, Schaper J, Schultheiss HP, Chien KR. The cardiac mechanical stretch sensor machinery involves a Z disc complex that is defective in a subset of human dilated cardiomyopathy. *Cell*. 2002;111:943–955.
- Olson TM, Michels VV, Thibodeau SN, Tai YS, Keating MT. Actin mutations in dilated cardiomyopathy, a heritable form of heart failure. *Science*. 1998;280:750–752.
- Towbin JA, Bowles NE. Genetic abnormalities responsible for dilated cardiomyopathy. *Curr Cardiol Rep*. 2000;2:475–480.
- Du CK, Morimoto S, Nishii K, Minakami R, Ohta M, Tadano N, Lu QW, Wang YY, Zhan DY, Mochizuki M, Kita S, Miwa Y, Takahashi-Yanaga F, Iwamoto T, Ohtsuki I, Sasaguri T. Knock-in mouse model of dilated cardiomyopathy caused by troponin mutation. *Circ Res*. 2007;101:185–194.
- Kawada T, Masui F, Tezuka A, Ebisawa T, Kumagai H, Nakazawa M, Toyo-Oka T. A novel scheme of dystrophin disruption for the progression of advanced heart failure. *Biochim Biophys Acta*. 2005;1751:73–81.
- Kyoi S, Otani H, Matsuhisa S, Akita Y, Tatsumi K, Enoki C, Fujiwara H, Imamura H, Kamihata H, Iwasaka T. Opposing effect of p38 MAP kinase and JNK inhibitors on the development of heart failure in the cardiomyopathic hamster. *Cardiovasc Res*. 2006;69:888–898.
- Olivetti G, Abbi R, Quaini F, Kajstura J, Cheng W, Nitahara JA, Quaini E, Di Loreto C, Beltrami CA, Krajewski S, Reed JC, Anversa P. Apoptosis in the failing human heart. *N Engl J Med*. 1997;336:1131–1141.
- Bulfield G, Siller WG, Wight PA, Moore KJ. X chromosome-linked muscular dystrophy (mdx) in the mouse. *Proc Natl Acad Sci U S A*. 1984;81:1189–1192.
- Cooper BJ, Winand NJ, Stedman H, Valentine BA, Hoffman EP, Kunkel LM, Scott MO, Fischbeck KH, Kornegay JN, Avery RJ, Williams JR, Schmickel RD, Sylvester JE. The homologue of the Duchenne locus is defective in X-linked muscular dystrophy of dogs. *Nature*. 1988;334:154–156.
- Nigro V, Okazaki Y, Belsito A, Piluso G, Matsuda Y, Politano L, Nigro G, Ventura C, Abbondanza C, Molinari AM, Acampora D, Nishimura M, Hayashizaki Y, Puca GA. Identification of the Syrian hamster cardiomyopathy gene. *Hum Mol Genet*. 1997;6:601–607.
- Tanaka M, Nakae S, Terry RD, Mokhtari GK, Gunawan F, Balsam LB, Kaneda H, Kofidis T, Tsao PS, Robbins RC. Cardiomyocyte-specific Bcl-2 overexpression attenuates ischemia-reperfusion injury, immune response during acute rejection, and graft coronary artery disease. *Blood*. 2004;104:3789–3796.
- Wilkins BJ, Dai YS, Bueno OF, Parsons SA, Xu J, Plank DM, Jones F, Kimball TR, Molkentin JD. Calcineurin/NFAT coupling participates in pathological, but not physiological, cardiac hypertrophy. *Circ Res*. 2004;94:110–118.
- Zhang R, Khoo MS, Wu Y, Yang Y, Grueter CE, Ni G, Price EE Jr, Thiel W, Guatimosim S, Song LS, Madu EC, Shah AN, Vishnivetskaya TA, Atkinson JB, Gurevich VV, Salama G, Lederer WJ, Colbran RJ, Anderson ME. Calmodulin kinase II inhibition protects against structural heart disease. *Nat Med*. 2005;11:409–417.
- Donehower LA, Harvey M, Slagle BL, McArthur MJ, Montgomery CA Jr, Butel JS, Bradley A. Mice deficient for p53 are developmentally normal but susceptible to spontaneous tumours. *Nature*. 1992;356:215–221.
- VanGuilder HD, Vrana KE, Freeman WM. Twenty-five years of quantitative PCR for gene expression analysis. *Biotechniques*. 2008;44:619–626.
- Olson TM, Doan TP, Kishimoto NY, Whitby FG, Ackerman MJ, Fananapazir L. Inherited and de novo mutations in the cardiac actin gene cause hypertrophic cardiomyopathy. *J Mol Cell Cardiol*. 2000;32:1687–1694.
- Wencker D, Chandra M, Nguyen K, Miao W, Garantziotis S, Factor SM, Shirani J, Armstrong RC, Kitsis RN. A mechanistic role for cardiac myocyte apoptosis in heart failure. *J Clin Invest*. 2003;111:1497–1504.
- Ryan KM, Phillips AC, Voudsen KH. Regulation and function of the p53 tumor suppressor protein. *Curr Opin Cell Biol*. 2001;13:332–337.
- Sano M, Minamino T, Toko H, Miyauchi H, Orimo M, Qin Y, Akazawa H, Tateno K, Kayama Y, Harada M, Shimizu I, Asahara T, Hamada H, Tomita S, Molkentin JD, Zou Y, Komuro I. p53-induced inhibition of Hif-1 causes cardiac dysfunction during pressure overload. *Nature*. 2007;446:444–448.
- Xiong S, Van Pelt CS, Elizondo-Fraire AC, Fernandez-Garcia B, Lozano G. Loss of Mdm4 results in p53-dependent dilated cardiomyopathy. *Circulation*. 2007;115:2925–2930.
- Hoch B, Meyer R, Hetzer R, Krause EG, Karczewski P. Identification and expression of delta-isoforms of the multifunctional Ca²⁺/calmodulin-dependent protein kinase in failing and nonfailing human myocardium. *Circ Res*. 1999;84:713–721.
- Zhang T, Johnson EN, Gu Y, Morissette MR, Sah VP, Gigena MS, Belke DD, Dillmann WH, Rogers TB, Schulman H, Ross J Jr, Brown JH. The cardiac-specific nuclear delta(B) isoform of Ca²⁺/calmodulin-dependent protein kinase II induces hypertrophy and dilated cardiomyopathy associated with increased protein phosphatase 2A activity. *J Biol Chem*. 2002;277:1261–1267.

26. Zhang T, Maier LS, Dalton ND, Miyamoto S, Ross J Jr, Bers DM, Brown JH. The deltaC isoform of CaMKII is activated in cardiac hypertrophy and induces dilated cardiomyopathy and heart failure. *Circ Res.* 2003;92:912-919.
27. Zhu WZ, Wang SQ, Chakir K, Yang D, Zhang T, Brown JH, Devic E, Kobilka BK, Cheng H, Xiao RP. Linkage of beta1-adrenergic stimulation to apoptotic heart cell death through protein kinase A-independent activation of Ca²⁺/calmodulin kinase II. *J Clin Invest.* 2003;111:617-625.
28. Peng W, Zhang Y, Zheng M, Cheng H, Zhu W, Cao CM, Xiao RP. Cardioprotection by CaMKII-deltaB is mediated by phosphorylation of heat shock factor 1 and subsequent expression of inducible heat shock protein 70. *Circ Res.* 2010;106:102-110.
29. Zhu W, Woo AY, Yang D, Cheng H, Crow MT, Xiao RP. Activation of CaMKIIdeltaC is a common intermediate of diverse death stimulus-induced heart muscle cell apoptosis. *J Biol Chem.* 2007;282:10833-10839.
30. Wu X, Zhang T, Bossuyt J, Li X, McKinsey TA, Dedman JR, Olson EN, Chen J, Brown JH, Bers DM. Local InsP3-dependent perinuclear Ca²⁺ signaling in cardiac myocyte excitation-transcription coupling. *J Clin Invest.* 2006;116:675-682.
31. Ling H, Zhang T, Pereira L, Means CK, Cheng H, Gu Y, Dalton ND, Peterson KL, Chen J, Bers D, Heller Brown J. Requirement for Ca²⁺/calmodulin-dependent kinase II in the transition from pressure overload-induced cardiac hypertrophy to heart failure in mice. *J Clin Invest.* 2009;119:1230-1240.

CLINICAL PERSPECTIVE

Heart failure is an important cause of morbidity and mortality in many industrial countries, and dilated cardiomyopathy (DCM) is one of its major causes. Molecular genetic studies over the last 2 decades have revealed many mutations of various genes in DCM patients, but the precise mechanisms of how such mutations lead to DCM remain largely unknown partly because of a lack of good animal models of DCM. Here, we established the mouse model of DCM by expressing a mutated cardiac α -actin gene, which has been reported in patients with DCM, in the heart. The transgenic mice showed gradual dilatation and dysfunction of the left ventricle, resulting in death by heart failure. These phenotypes of the transgenic mice were quite similar to those of human DCM. The number of apoptotic cardiomyocytes and protein levels of p53 were increased in the hearts of the DCM mice. Overexpression of Bcl-2, an antiapoptotic factor, or downregulation of p53 decreased the number of apoptotic cardiomyocytes and improved cardiac function. The DCM mice showed activation of CaMKII δ . The inhibition of CaMKII δ prevented the increase in p53 and apoptotic cardiomyocytes and ameliorated cardiac function. These results suggest that CaMKII δ plays a critical role in the development of heart failure in part by accumulation of p53 and induction of cardiomyocyte apoptosis in the DCM mouse model. The inhibition of CaMKII δ may become a new therapeutic strategy for DCM patients.



Sonic hedgehog is a critical mediator of erythropoietin-induced cardiac protection in mice

Kazutaka Ueda,¹ Hiroyuki Takano,¹ Yuriko Niitsuma,^{1,2} Hiroshi Hasegawa,¹ Raita Uchiyama,¹ Toru Oka,¹ Masaru Miyazaki,² Haruaki Nakaya,³ and Issei Komuro¹

¹Department of Cardiovascular Science and Medicine, ²Department of General Surgery, and ³Department of Pharmacology, Chiba University Graduate School of Medicine, Chiba, Japan.

Erythropoietin reportedly has beneficial effects on the heart after myocardial infarction, but the underlying mechanisms of these effects are unknown. We here demonstrate that sonic hedgehog is a critical mediator of erythropoietin-induced cardioprotection in mice. Treatment of mice with erythropoietin inhibited left ventricular remodeling and improved cardiac function after myocardial infarction, independent of erythropoiesis and the mobilization of bone marrow-derived cells. Erythropoietin prevented cardiomyocyte apoptosis and increased the number of capillaries and mature vessels in infarcted hearts by upregulating the expression of angiogenic cytokines such as VEGF and angiopoietin-1 in cardiomyocytes. Erythropoietin also increased the expression of sonic hedgehog in cardiomyocytes, and inhibition of sonic hedgehog signaling suppressed the erythropoietin-induced increase in angiogenic cytokine expression. Furthermore, the beneficial effects of erythropoietin on infarcted hearts were abolished by cardiomyocyte-specific deletion of sonic hedgehog. These results suggest that erythropoietin protects the heart after myocardial infarction by inducing angiogenesis through sonic hedgehog signaling.

Introduction

Recent medical advances have improved survival rates of patients with acute myocardial infarction (MI), whereas the number of patients showing heart failure after MI has increased in recent years (1). LV remodeling, which includes dilatation of the ventricle and increased interstitial fibrosis, is the critical process that underlies the progression to heart failure (1). Although pharmacological therapies are effective, heart failure is still one of the leading causes of death worldwide (2). It is thus important to elucidate a novel approach to prevent LV remodeling after MI.

Several hematopoietic cytokines including erythropoietin (EPO), G-CSF, and stem cell factor have been reported to prevent cardiac remodeling and dysfunction after MI in various animal models (3–5). EPO, a major regulator of erythroid progenitors, has attracted great attention because its administration induced significant improvements in the clinical status and LV function of patients with congestive heart failure (6, 7). Although several mechanisms of cardioprotective effects by EPO have been suggested, the precise mechanisms remain largely unknown (8–14). Treatment with EPO reverses the decreased oxygen-carrying capacity associated with anemia, which is often observed in patients with heart failure (8). EPO has also been reported to mobilize endothelial progenitor cells (EPCs) from bone marrow, leading to neovascularization in the heart (9). In addition, since EPO receptors (EPORs) are expressed in various types of cells including cardiomyocytes, EPO may have direct protective effects on cardiomyocytes (10–14).

In the present study, we investigated the mechanisms of how EPO induced cardioprotection after MI. We observed that EPO directly

prevented apoptotic death of cardiomyocytes and enhanced the expression of angiogenic cytokines, which induced robust angiogenesis, leading to the improvement of contractile function after MI. EPO also increased expression levels of sonic hedgehog (Shh) in cardiomyocytes, and the inhibition of Shh signaling abolished the EPO-induced increases of angiogenic cytokine production in cardiomyocytes. In hearts of cardiac-specific inducible Shh knock-out (Shh-MerCre) mice, EPO treatment failed to upregulate angiogenic cytokines, enhance angiogenesis, and inhibit LV remodeling. Our results suggest that Shh is a key mediator of EPO-evoked cardioprotection in infarcted hearts.

Results

EPO prevents cardiac remodeling after MI. We subcutaneously administered EPO (10,000 U/kg/d) or saline immediately after coronary artery ligation until 4 days after MI. Fourteen days after MI, we histologically assessed the infarct size and examined cardiac function using echocardiography. Treatment with EPO significantly prevented enlargement of LV end-diastolic dimension (LVEDD) and reduction of fractional shortening (FS) and reduced the infarct size (fibrotic area/LV free wall) compared with saline treatment (Figure 1, A and B), suggesting that EPO prevents LV remodeling and dysfunction after MI.

The role of hematopoietic effects of EPO in cardioprotection (6, 7) was examined using transgene-rescued EPOR-null (RES) mice, which express EPORs only in the hematopoietic lineage (15). Although EPO treatment increased blood hemoglobin levels 7 days after MI in both WT and RES mice (Figure 2A), the cardioprotective effects of EPO were observed only in WT mice but not in the RES mice (Figure 1 and Figure 2B). EPO and saline did not show any significant differences in LVEDD, FS, or infarct size in the RES mice (Figure 2B), suggesting that erythropoiesis is not involved in the cardioprotective effects of EPO.

Authorship note: Kazutaka Ueda, Hiroyuki Takano, and Yuriko Niitsuma contributed equally to this work.

Conflict of interest: The authors have declared that no conflict of interest exists.

Citation for this article: *J Clin Invest.* 2010;120(6):2016–2029. doi:10.1172/JCI39896.

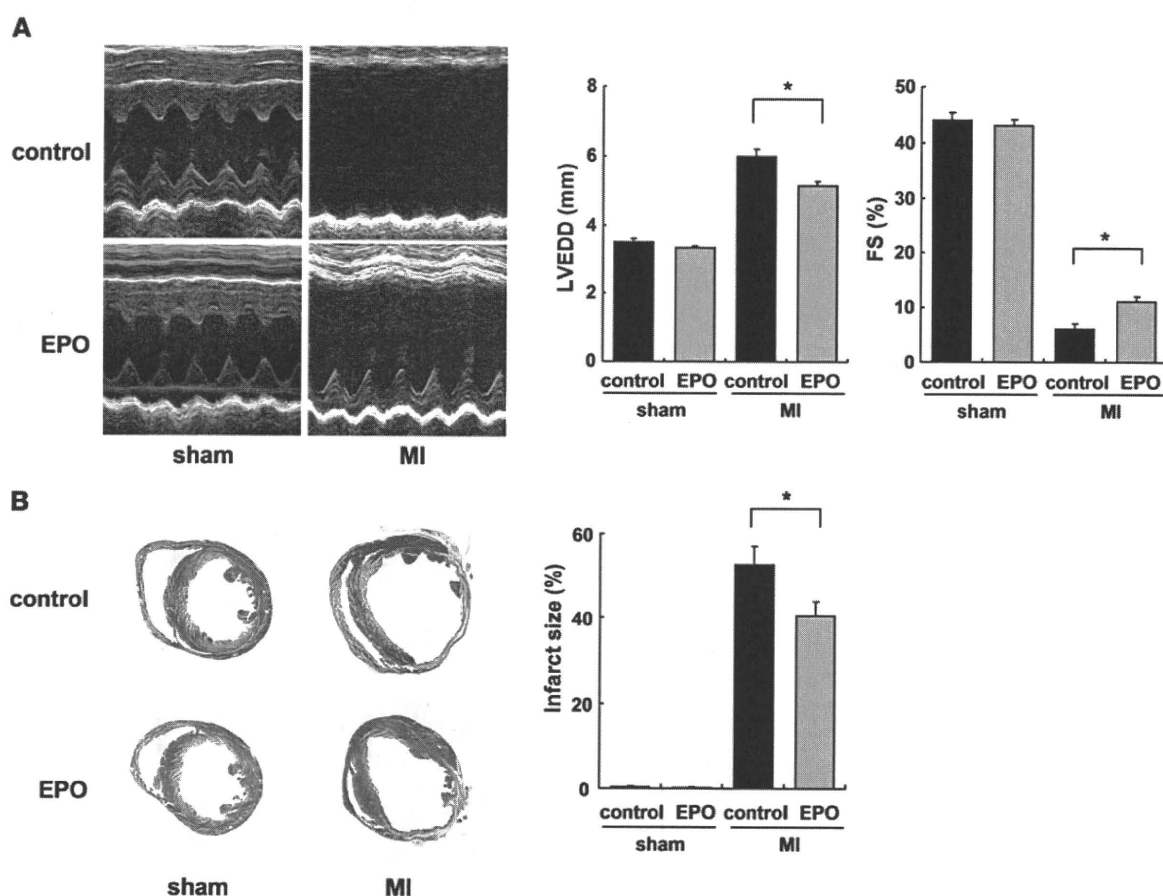


Figure 1

EPO prevents cardiac remodeling after MI. The effects of EPO treatment on LV function and infarct size were examined 14 days after operation. WT mice were subjected to MI or sham operation and treated with EPO or saline (control). (A) Echocardiographic analysis. ($n = 8-10$). (B) Masson trichrome staining of hearts and infarct size ($n = 8-10$). $*P < 0.01$.

To investigate whether EPO affects responses of inflammation and wound healing that may have an impact on LV remodeling after MI (16, 17), we examined macrophage infiltration and myofibroblast accumulation in the ischemic area after MI by immunohistochemical staining. The number of Mac3-positive macrophages was markedly decreased by EPO treatment 14 days after MI (Supplemental Figure 1A; supplemental material available with this article; doi:10.1172/JCI39896DS1). The number of α -SMA-positive myofibroblasts was significantly increased in EPO-treated hearts compared with saline-treated hearts (Supplemental Figure 1B).

We next determined whether EPO induced the mobilization of EPCs from bone marrow into peripheral blood using flow cytometry (9). After MI, EPO significantly increased the number of circulating CD34/Flk-1-double-positive EPCs in WT mice but not in the RES mice (Figure 2C). We produced MI in WT mice in which the bone marrow was replaced with cells derived from GFP-expressing mice. The hearts were excised 7 and 14 days after MI and immunohistochemically stained for PECAM. There were no differences in the number of GFP-positive cells and GFP/PECAM-double-positive cells in the border areas of EPO- and saline-treated infarcted hearts (Figure 2D), indicating that EPO did not enhance the homing of bone marrow-derived cells or increase the number of bone marrow-derived endothelial cells in the damaged hearts, although

EPO induced mobilization of EPCs from bone marrow into peripheral circulation. In addition, EPO did not improve cardiac function or increase the number of vessels in infarcted hearts even in RES mice transplanted with bone marrow of WT mice (Figure 2E). It is thus unlikely that the EPO-mobilized bone marrow-derived cells contribute to the cardioprotective effects of EPO.

EPO inhibits cardiomyocyte apoptosis in infarcted hearts. Apoptotic death of cardiomyocytes has been suggested to cause LV remodeling and dysfunction (18). To determine the role of antiapoptotic effects of EPO in cardioprotection, we performed TUNEL staining of hearts 24 hours after MI. The number of TUNEL-positive cardiomyocytes in the border area was significantly smaller in EPO-treated mice than in saline-treated mice, while EPO treatment had no effect on cardiomyocyte apoptosis in RES mice (Figure 3A). Western blot analysis showed that EPO treatment markedly reduced the level of cleaved caspase-3 in hearts at 24 hours after MI (Figure 3B). TUNEL staining revealed that pretreatment with EPO significantly attenuated H_2O_2 -induced apoptotic death in cultured cardiomyocytes of neonatal rats (Figure 3C). At 24 hours after exposing cardiomyocytes to H_2O_2 , expression levels of the antiapoptotic protein Bcl-2 were decreased, whereas levels of cleaved caspase-3 were increased, and these changes were inhibited markedly by EPO pretreatment (Figure 3D). Annexin V staining

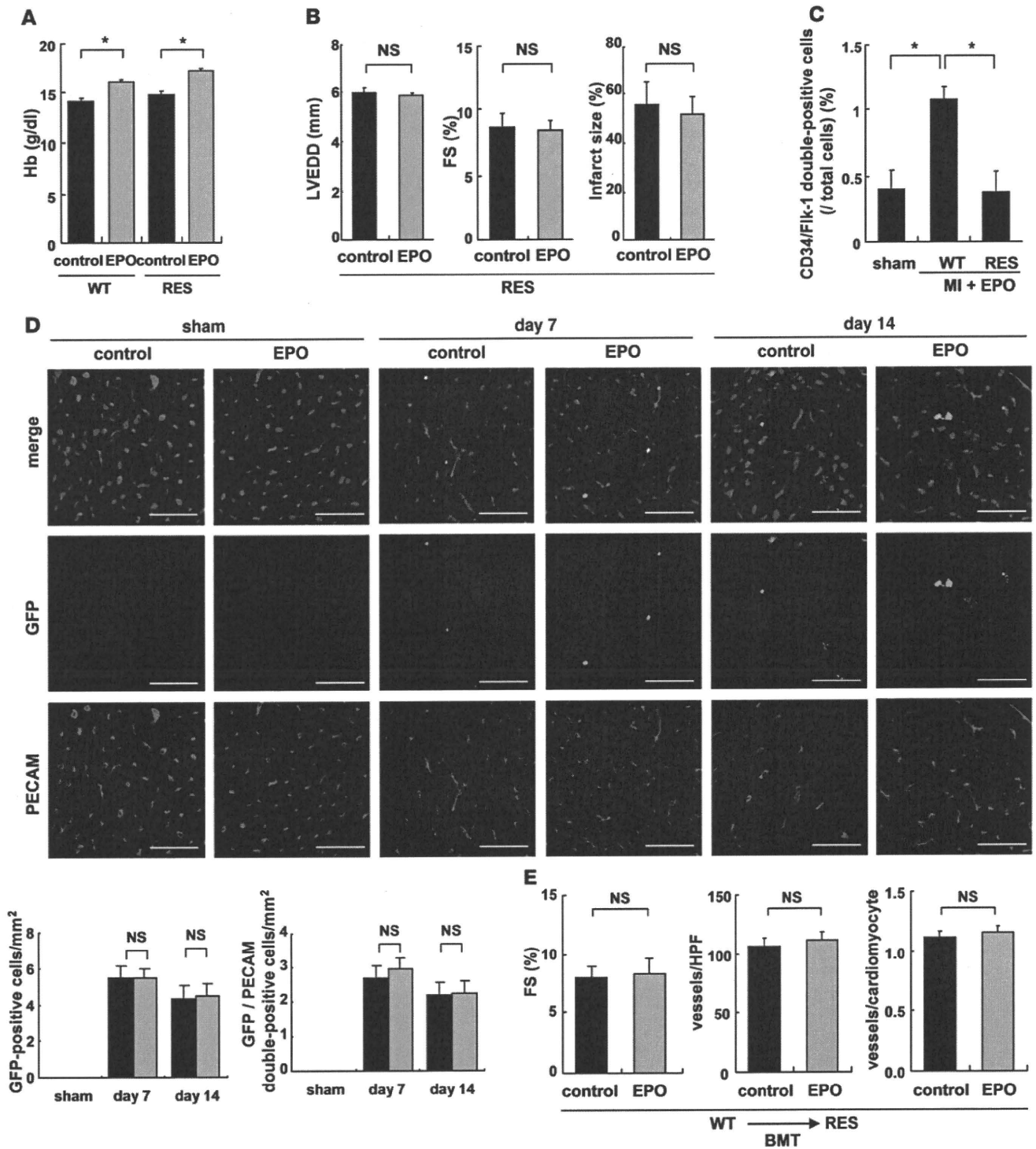


Figure 2

Erythroid hematogenesis is not required for the protective effects of EPO, and EPO does not accelerate the cardiac homing of bone marrow-derived cells after MI. WT and RES mice were subjected to MI and treated with EPO or saline (control). (A) Blood hemoglobin (Hb) levels 7 days after MI ($n = 4$). $*P < 0.01$. (B) Echocardiography and Masson trichrome staining were performed to analyze LV function and infarct size ($n = 10$). (C) Following MI and EPO treatment, the number of circulating CD34/Fli-1–double-positive EPCs increased in WT mice but not in RES mice. $*P < 0.05$ ($n = 4$). (D) Bone marrow cells from GFP-expressing mice were transplanted into WT mice. 7 and 14 days after MI, immunohistochemical staining for PECAM (red) was performed, and nuclei were counterstained with TO-PRO-3 (blue). GFP-positive cells (green) represent bone marrow–derived cells that moved into the heart and GFP/PECAM–double-positive cells denote bone marrow–derived endothelial cells. The numbers of GFP– and GFP/PECAM–double-positive cells in the border area (MI group) or LV free wall (sham group) were counted ($n = 5–8$). Scale bars: 50 μm . (E) WT bone marrow cells were transplanted (BMT) into RES mice, MI was induced, and the mice were treated with EPO or saline (control). FS, the number of vessels, and the ratio of vessels to cardiomyocytes in the border area are shown ($n = 8$).

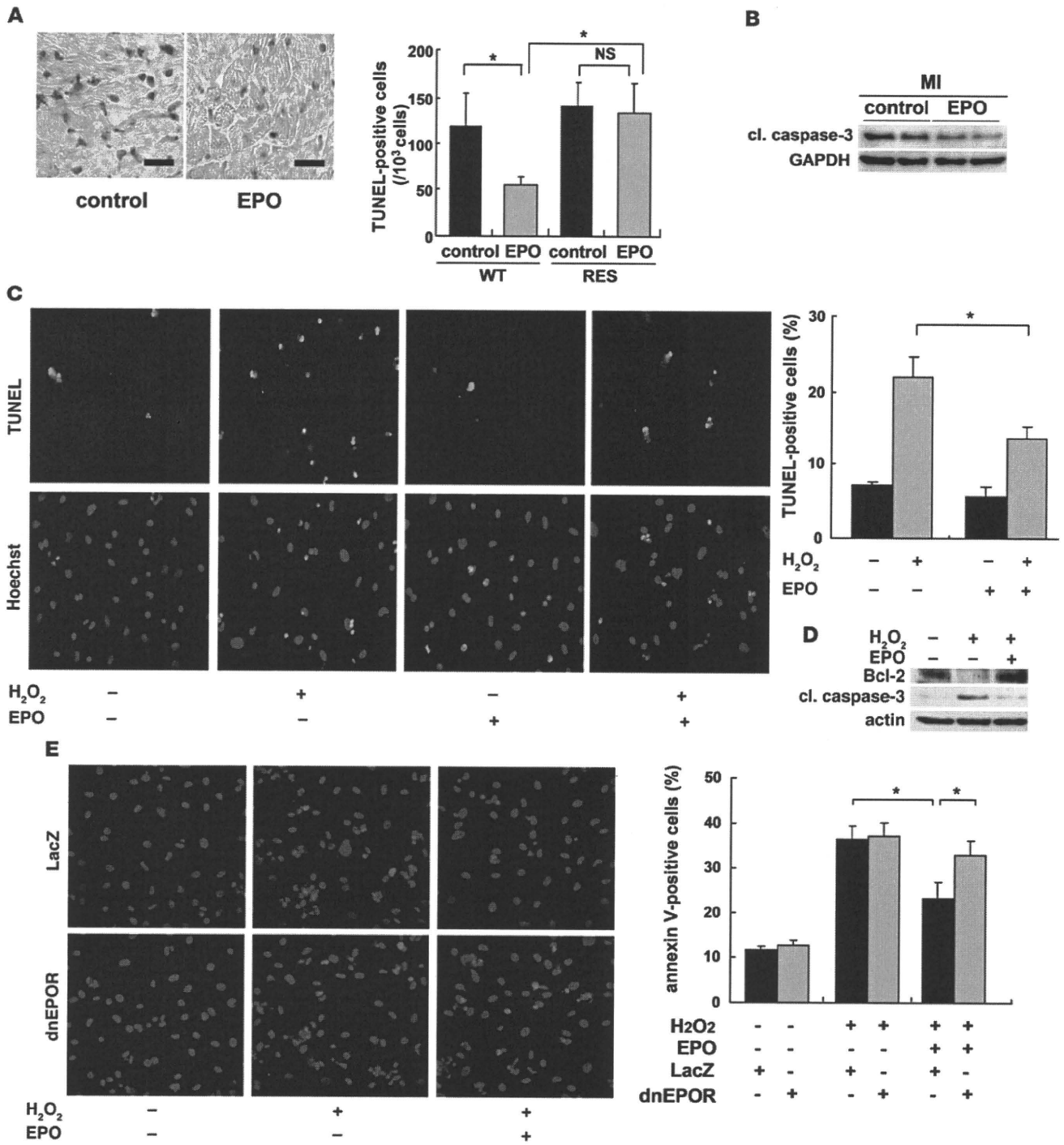
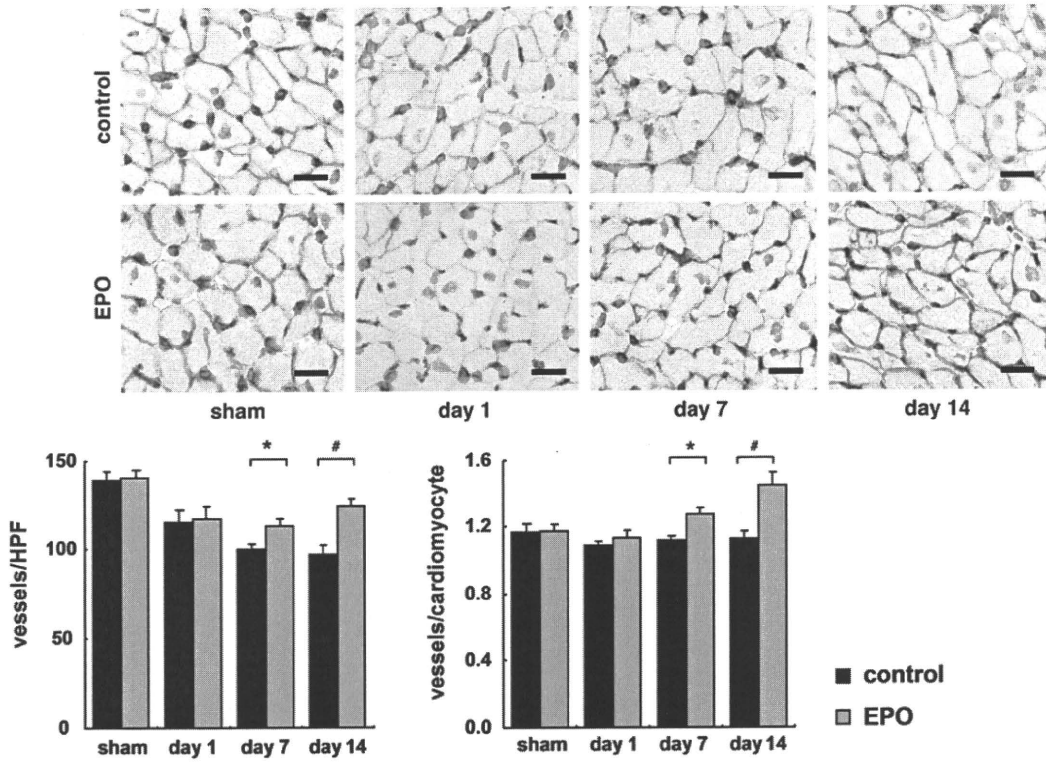


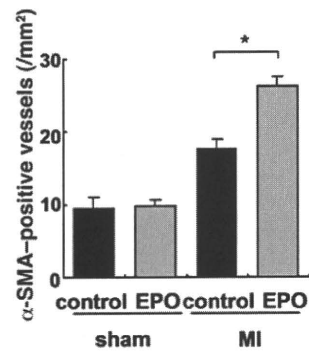
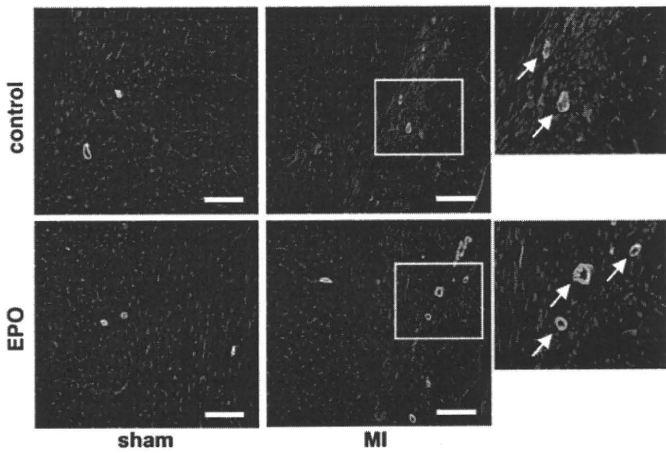
Figure 3 EPO inhibits cardiomyocyte apoptosis in infarcted hearts. (A) TUNEL staining (brown) of infarcted hearts from WT mice 24 hours after ligation. Scale bars: 100 μm. The number of TUNEL-positive cardiomyocytes in the border area was counted. **P* < 0.01 (*n* = 10). (B) Representative Western blots of cleaved caspase-3 (cl. caspase-3) protein in the heart 24 hours after MI are shown (*n* = 4). (C) Detection of apoptotic cardiomyocytes using FITC-labeled TUNEL staining (green). Nuclei were counterstained with Hoechst 33258 (blue). The TUNEL-positive cardiomyocytes were counted (*n* = 10). **P* < 0.05. (D) Samples were pretreated with EPO for 8 hours before H₂O₂ treatment, and the expression of Bcl-2 and cleaved caspase-3 24 hours after H₂O₂ treatment was analyzed by Western blotting. Representative results from 3 experiments are shown. (E) Detection of apoptotic cardiomyocytes using Cy-3-labeled annexin V staining (red). Nuclei were counterstained with Hoechst 33258 (blue). Cardiomyocytes were infected with adenoviral vectors encoding dominant negative form of EPOR or LacZ at 10 MOI. The number of annexin V-positive cardiomyocytes was counted (*n* = 10). **P* < 0.05.



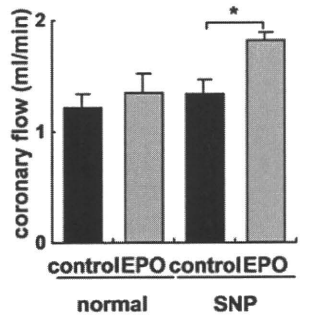
A



B



C



D

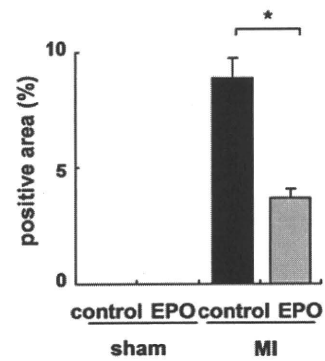
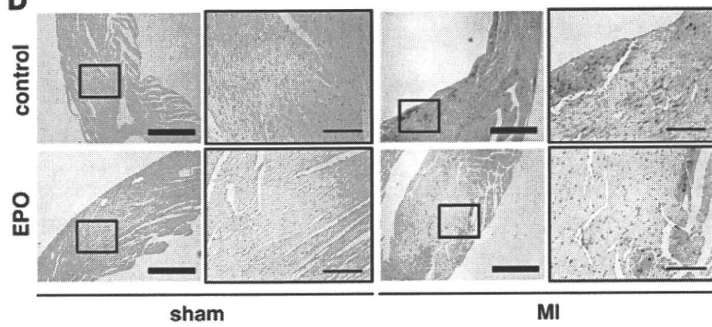


**Figure 4**

EPO promotes angiogenesis in infarcted hearts. (A) Double immunostaining for PECAM (green) and dystrophin (brown) in the border area (MI group) or LV free wall (sham group) of EPO- and saline-treated (control) hearts. Scale bars: 20 μm . The number of vessels and the ratio of vessels to cardiomyocyte were measured ($n = 8$ for each). * $P < 0.05$; # $P < 0.01$. (B) Double immunohistochemical staining for α SMA (green) and PECAM (red) shown together with TO-PRO-3 (blue) staining in the border area (MI group) or LV free wall (sham group) 14 days after operation. The number of α -SMA-positive vessels in the ischemic area was determined ($n = 8$). Scale bars: 100 μm . * $P < 0.05$. (C) Coronary flow was measured in EPO- and saline-treated (control) hearts 14 days after MI with or without sodium nitroprusside (SNP, 10^{-4} M) ($n = 6$). * $P < 0.05$. (D) Representative images of hypoxyprobe staining (brown) of EPO- and saline-treated (control) hearts in the border area (MI group) or LV free wall (sham group) 7 days after operation. The rate of hypoxyprobe-positive area in the border area was measured ($n = 3$). Scale bars: 500 μm (thick bars); 100 μm (thin bars). * $P < 0.01$.

showed that EPO-induced antiapoptotic effects were abolished by transducing adenoviral vectors, which encode the dominant negative form of EPOR (Figure 3E). These results suggest that EPO accomplishes antiapoptotic effects on cardiomyocytes through the EPO/EPOR signaling pathways. EPO has been reported to activate several kinases including Akt and ERK, which promote cell surviving pathways (10, 19). We thus determined whether EPO inhibits the death of cardiomyocytes by activating these kinases. Indeed, both Akt and ERK were activated in cultured cardiomyocytes by EPO in a time- and dose-dependent manner, and these activations were abolished by transducing dominant negative EPOR (Supplemental Figure 2, A–C). Inhibitions of Akt and ERK using respective kinase inhibitors suppressed EPO-induced reduction in the number of TUNEL-positive cardiomyocytes and EPO-induced downregulation of cleaved caspase-3 (Supplemental Figure 2, D and E), suggesting that EPO prevents apoptotic death of cardiomyocytes at least in part by activating Akt and ERK through the EPO/EPOR system in cardiomyocytes.

Angiogenic cytokines mediate EPO-induced cardioprotection. To determine the angiogenic effects of EPO, we performed immunohistochemical double-staining of infarcted hearts for PECAM and dystrophin. EPO treatment markedly increased the number of PECAM-positive capillary vessels and the ratio of vessels to cardiomyocytes in the border area at 7 days after MI (Figure 4A). Moreover, EPO significantly increased the number of α -SMA-positive vessels in the heart 14 days after MI (Figure 4B), suggesting that EPO induces the formation of mature vessels in infarcted hearts.

We also investigated the effects of EPO-induced angiogenesis on myocardial perfusion. At 14 days after MI, the coronary flow under dilatory stimulation with sodium nitroprusside was significantly increased in EPO-treated hearts compared with saline-treated hearts in the isolated heart perfusion system (Figure 4C). The extent of myocardial ischemia in the border area detected by Hypoxyprobe staining was decreased by EPO treatment (Figure 4D), suggesting that EPO-induced angiogenesis is functionally relevant to the enhancement of coronary perfusion reserve and the reduction of cardiac ischemia in infarcted hearts. Meanwhile, there were no significant differences in the cross-sectional area of cardiomyocytes in the border area at 14 days after MI between EPO and saline treatment (Supplemental Figure 3).

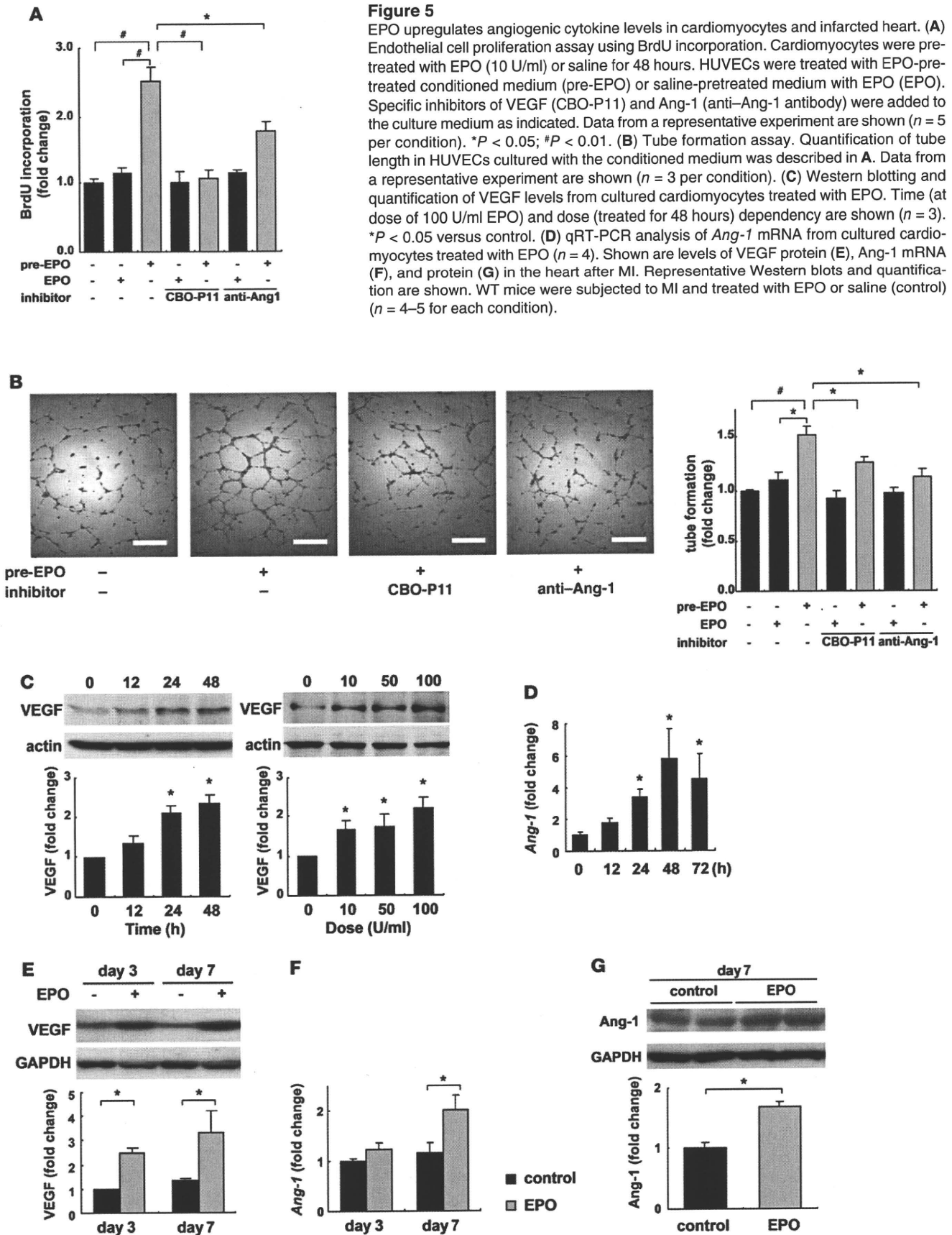
We also examined the mechanisms of EPO-induced angiogenesis in vitro using HUVECs. The administration of EPO did not increase BrdU incorporation into HUVECs. In contrast, the culture medium of cardiomyocytes conditioned by EPO markedly enhanced the BrdU incorporation into HUVECs compared with the cultured medium of cardiomyocytes conditioned by saline (Figure 5A). The conditioned medium from EPO-treated cardiomyocytes also significantly enhanced tube formation of HUVECs, whereas the administration of EPO itself did not affect tube formation of HUVECs cultured in the medium from saline-treated cardiomyocytes (Figure 5B). These results suggest that EPO evokes an angiogenic response by inducing paracrine factors secreted from cardiomyocytes.

EPO upregulated the levels of VEGF in cultured cardiomyocytes in both time- and dose-dependent manners (Figure 5C). EPO also upregulated the levels of angiopoietin-1 (*Ang-1*) mRNA in cardiomyocytes, as evidenced by quantitative RT-PCR (qRT-PCR) (Figure 5D). Proliferation and tube formation of HUVEC induced by the conditioned medium from EPO-treated cardiomyocytes were significantly suppressed by a VEGF-specific inhibitor (CBO-P11) or an anti-Ang-1 antibody (Figure 5, A and B). Additionally, when VEGF was knocked down in cardiomyocytes using siRNA, the EPO-induced proliferation of HUVECs was also suppressed (Supplemental Figure 4A). These results suggest that VEGF and Ang-1 secreted from cardiomyocytes mediate the EPO-induced angiogenic response.

Consistent with the in vitro results, EPO treatment markedly increased the levels of VEGF and Ang-1 proteins and *Ang-1* mRNA in the heart after MI (Figure 5, E–G). To determine the role of EPO-mediated VEGF expression in vivo, we injected an adenoviral vector encoding a soluble form of Flt-1, an inhibitor of VEGF, into the thigh muscles of WT mice 4 days before and 3 days after MI. The beneficial effects of EPO on infarcted hearts, including increased vessel number, reduced infarct size, and improved cardiac function, were all abolished by VEGF inhibition (Figure 6), suggesting that VEGF secreted from cardiomyocytes plays a critical role in the cardioprotective effects of EPO against MI.

Shh is a critical mediator of the angiogenic effects of EPO. We further investigated how EPO increases angiogenic cytokine levels in infarcted hearts. Since Akt and ERK, which are activated by EPO, have been reported to regulate VEGF expression (19, 20), we first determined whether EPO increased expression levels of VEGF by activating these kinases in cardiomyocytes. Although both Akt and ERK were activated by EPO in cultured cardiomyocytes, activation levels were not so high as compared with other growth factors such as insulin (Supplemental Figure 2B and data not shown). Since EPO-induced upregulation of VEGF was so robust, we hypothesized that other mitogens mediate the EPO-induced upregulation of VEGF. It has recently been reported that carbamylated EPO (CEPO) promotes neural progenitor cell proliferation and their differentiation into neurons through an upregulation of Shh expression (21). Shh, a critical regulator of patterning and growth in various tissues during embryogenesis, has been reported to show angiogenic effects in infarcted hearts (22, 23). We thus examined the involvement of Shh signaling in EPO-induced cardioprotection.

To determine whether EPO upregulates Shh expression in cardiomyocytes, we first examined the levels of Shh in cultured cardiomyocytes. Both EPO and CEPO induced a marked accumulation of the biologically active, aminoterminal fragment of Shh



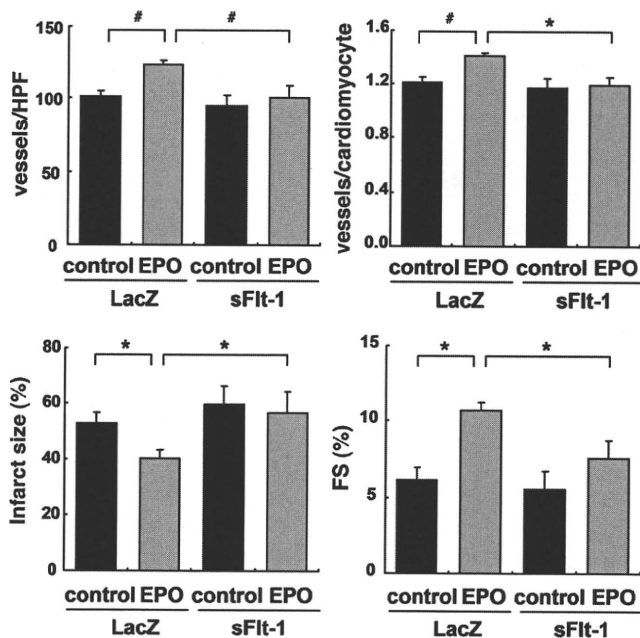


Figure 6

VEGF is essential for the angiogenic and cardioprotective effects of EPO. WT mice were injected with adenoviral vectors encoding soluble Fit-1 (sFit-1) or LacZ, subjected to MI, and treated with EPO or saline (control). Echocardiographic analysis and immunohistochemical staining were then performed ($n = 8$). * $P < 0.05$; # $P < 0.01$.

(Shh-N) in cardiomyocytes but not in cardiac fibroblasts 48 hours after treatment (Figure 7A), and Shh-N was abundantly secreted from EPO-treated cardiomyocytes into the culture medium (Figure 7B). Immunocytochemical analysis demonstrated that EPO induced the accumulation of Shh in α -sarcomeric actinin-positive cardiomyocytes but not in vimentin-positive cardiac fibroblasts (Figure 7C). In addition, EPO treatment significantly upregulated the levels of *Shh* mRNA in cardiomyocytes (Figure 7D).

We next determined whether Shh augmented angiogenic cytokine levels in cultured cardiomyocytes. Addition of recombinant murine Shh-N peptide (rmShh) increased the mRNA levels of the downstream target genes *Ptch1* and *Gli1* in cardiomyocytes in a dose-dependent manner (Figure 7E). rmShh also increased the levels of VEGF protein and *Ang-1* mRNA in cardiomyocytes as well as the concentration of VEGF protein in the culture medium (Figure 7, E and F). These changes were blocked by cyclopamine, a specific inhibitor of Shh signaling (Figure 7, E and F).

Cyclopamine treatment also significantly inhibited the EPO-induced increases in the levels of VEGF protein and *Ang-1* mRNA (Figure 8, A and B). Moreover, cyclopamine significantly inhibited the proliferation of HUVEC induced by conditioned medium from cardiomyocytes pretreated with EPO (Figure 8C). Consistently, knockdown of Shh in cardiomyocytes also inhibited the EPO-induced proliferation of HUVEC (Supplemental Figure 4B), indicating that EPO induces expression of angiogenic cytokines by activating Shh signaling in cardiomyocytes.

On the other hand, the EPO-induced inhibition of cardiomyocyte apoptosis 24 hours after exposure to H_2O_2 was not affected by cyclopamine (Figure 8D), suggesting that EPO shows its antiapoptotic effects on cardiomyocytes through a Shh-independent pathway.

Cardiomyocyte-specific Shh deletion abolishes EPO-induced cardioprotection. We next determined the role of Shh signaling in EPO-induced cardioprotection in vivo. The expression levels of Shh and Patched were increased in infarcted hearts (Figure 9A), as previously reported (23). Notably, expression levels of Shh and Patched protein were higher in infarcted hearts treated with EPO than in those treated with saline (Figure 9A), indicating that EPO activates Shh signaling in infarcted hearts. Meanwhile, there were no differences in the expression levels of Shh protein in the infarcted hearts of WT and RES mice, suggesting that endogenous EPO signaling is not associated with the upregulation of Shh in the infarcted hearts (Supplemental Figure 5).

Systemic deletion of Shh has been reported to result in cardiovascular defects in mice (24). To elucidate the roles of EPO-induced activation of Shh signaling pathways in infarcted hearts, we employed Shh-MerCre mice in which Shh is deleted only in cardiomyocytes following tamoxifen treatment. We crossed *Shh^{floxed/floxed}* mice (25) with the transgenic mice in which a transgene encoding Cre recombinase was fused to the mutated estrogen receptor domains (MerCreMer) driven by the cardiomyocyte specific α -myosin heavy chain (α -MHC) promoter (26), and then produced the MHC-MerCreMer; *Shh^{floxed/floxed}* mutant (Shh-MerCre) mice. After tamoxifen treatment, we confirmed that EPO-induced increases in the expression levels of Shh protein were significantly attenuated in the infarcted hearts of Shh-MerCre mice (Figure 9B). Under basal conditions at 7 days after tamoxifen treatment and at 14 days after MI, there were no significant differences in LV function or the number of vessels and the ratio of vessels to cardiomyocytes among Shh-MerCre mice, *Shh^{floxed/floxed}* mice, MHC-MerCreMer mice, and WT mice (Figure 9, C and D, and data not shown).

There were no significant differences in LVEDD, FS, and infarct size in the Shh-MerCre mice treated with or without EPO after MI (Figure 9C). EPO did not increase the number of vessels, the ratio of vessels to cardiomyocytes, and the number of α -SMA-positive vessels in Shh-MerCre mice (Figure 9D). EPO treatment also failed to upregulate VEGF protein and *Ang-1* mRNA levels in Shh-MerCre mice (Figure 9, E and F), suggesting that myocardial Shh signaling is critical for the angiogenic and cardioprotective effects of EPO in infarcted hearts.

The role of STAT3 in the mechanism of EPO-induced cardioprotection. We have recently reported that G-CSF prevents LV remodeling after MI through the JAK2/STAT3 pathway in cardiomyocytes (5). To determine whether STAT3 is also involved in cardioprotective effects of EPO, we produced an MI model in transgenic mice that express dominant negative STAT3 in cardiomyocytes under the control of the α -MHC promoter (dnSTAT3-Tg). In dnSTAT3-Tg mice, the EPO treatment reduced infarct size and ameliorated LV dysfunction and remodeling at 14 days after MI by the same degree as WT mice (Supplemental Figure 6A). Overexpression of dnSTAT3 had no effects on EPO-induced prevention of H_2O_2 -induced apoptotic death in cardiomyocytes (Supplemental Figure 6B), indicating that STAT3 is not involved in the mechanism of EPO-induced cardioprotective effects after MI.

Discussion

In the present study, we elucidated what we believe are novel mechanisms underlying the EPO-mediated inhibition of cardiac remodeling after MI. EPO enhanced the expression of angiogenic cytokines such as VEGF and *Ang-1* in cultured cardiomyocytes and infarcted hearts, which, in turn, induced the proliferation of vas-

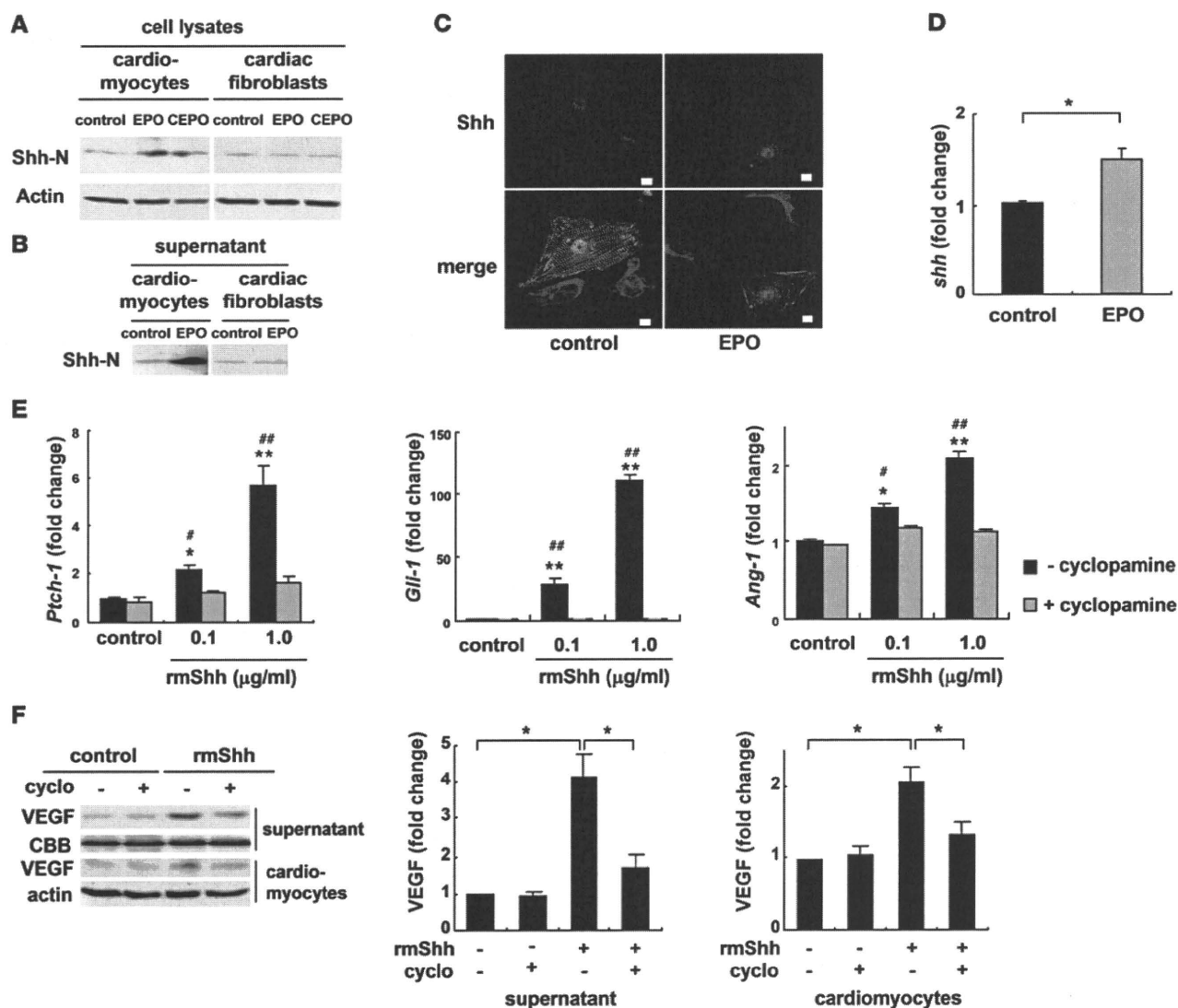


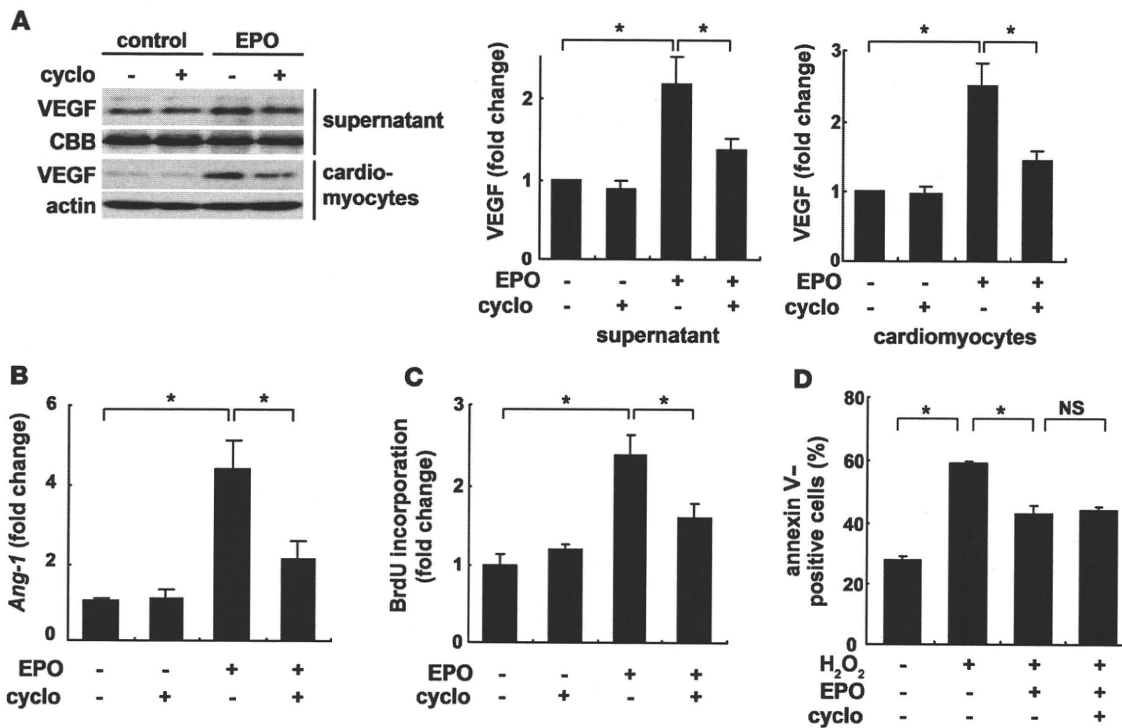
Figure 7

EPO upregulates expression levels of Shh. Western blotting of Shh in cultured neonatal rat cardiomyocytes and cardiac fibroblasts (A) and in the culture supernatants (B). Cells were treated with EPO (100 U/ml) or CEPO (100 U/ml) for 48 hours. Shh-N represents the aminoterminal domain of Shh, which is a biologically active form of Shh. (C) Immunocytochemical staining for Shh (red), α -sarcomeric actinin (green), and vimentin (blue). Cardiomyocytes and cardiac fibroblasts were cocultured with or without EPO for 48 hours. EPO induced the cytoplasmic accumulation of Shh in cardiomyocytes but not cardiac fibroblasts. Scale bars: 10 μ m. (D) qRT-PCR analysis of *Shh* mRNA. Cardiomyocytes were treated with EPO for 24 hours ($n = 5$). * $P < 0.05$. (E) qRT-PCR analysis of *Ptch-1*, *Gli-1*, and *Ang-1* mRNA. Cardiomyocytes were treated with rmShh (0.1 or 1.0 μ g/ml) for 24 hours ($n = 4$). * $P < 0.05$; ** $P < 0.01$ versus control. # $P < 0.05$; ## $P < 0.01$ versus rmShh and cycloamine (5 μ M) treatment. (F) Western blotting of VEGF. Cardiomyocytes were treated with rmShh (1.0 μ g/ml) for 48 hours. Cycloamine (cyclo) was administered 15 minutes before rmShh treatment. Representative Western blots and quantification of the bands are shown ($n = 4$).

cular endothelial cells and angiogenesis. EPO also increased Shh levels in cardiomyocytes, and the various effects evoked by EPO were attenuated by inhibiting Shh signaling (Figure 9G).

We found that EPO promoted angiogenesis by upregulating the expression of VEGF and Ang-1. VEGF is a key molecule that initiates proliferation and migration of endothelial cells and promotes the formation of new vessels, whereas chronic VEGF overexpression in mice has been reported to produce numerous small vessels lacking functional layers (27). Ang-1 induces recruitment of smooth muscle cells to primitive vessels consisting of endothelial cells (27–29). Therefore, our results suggest that EPO

treatment might be a better approach to creating stable and functional vessels in infarcted myocardium than the treatment with single angiogenic cytokine. Inhibition of angiogenesis by using the inhibitor of VEGF significantly attenuated the protective effects of EPO, such as the reduction of infarct size and improvement of LV function after MI. Since sufficient coronary perfusion resulting from angiogenesis can prevent cardiomyocyte apoptosis and improve contractile function (30, 31), angiogenic effects as well as direct antiapoptotic effects of EPO might protect the heart after MI. In this study, EPO did not enhance the homing of bone marrow-derived cells in damaged hearts, although EPO induced

**Figure 8**

Shh is a critical mediator of the angiogenic effects of EPO *in vitro*. The expression levels of VEGF protein (A) and *Ang-1* mRNA (B). Cardiomyocytes were treated with EPO for 48 hours. Cyclophamide (5 μ M) was added before EPO treatment. Quantification of the bands is shown ($n = 4$). * $P < 0.05$. (C) HUVEC proliferation assay. HUVECs were treated with cardiomyocyte-conditioned medium. Cyclophamide was added before EPO treatment. $n = 5$ per condition. (D) Detection of apoptosis using Cy3-labeled annexin V. Quantitative analysis is shown ($n = 6$).

mobilization of bone marrow cells including EPCs from bone marrow into peripheral circulation. It was previously reported that intramyocardial gene transfer of Shh enhanced angiogenesis by bone marrow-derived endothelial cells (23). Although reasons for the different results are not clear at present, the discrepancy may come from expression levels of Shh. Expression levels of Shh produced by intramyocardial gene transfer might be much higher than those induced by subcutaneous injection of EPO, and mode of actions of Shh (i.e., autocrine, paracrine, and endocrine) may be dependent on the expression levels of Shh.

EPO upregulated expression of Shh in cardiomyocytes, which played a critical role in protection of the heart after MI by increasing angiogenic cytokine production. In infarcted hearts, expression levels of Shh and its downstream target Patched have been reported to be increased (23), and Shh has been shown to produce robust angiogenic effects (22, 23). A recent study has demonstrated that cardiomyocyte-specific deletion of *Smoothened*, an essential component of Shh signaling, reduces the expression of angiogenic genes and the number of coronary vessels, resulting in cardiomyocyte apoptosis and cardiac dysfunction, and that vascular smooth muscle cell-specific deletion of *Smoothened* does not affect angiogenesis and cardiac function (32). These results and observations suggest that Shh upregulated by EPO in cardiomyocytes acts on cardiomyocytes themselves in an autocrine manner and increases production of angiogenic cytokines. There were no significant differences in size and function of LV and infarct size among the Shh-MerCre mice, *Shh^{floxex/floxex}* mice, and MHC-MerCre mice without EPO after MI. It has been demonstrated

that hedgehog, which is produced mainly by fibroblasts, is critical for maintenance and survival of the coronary vasculature in the adult heart and that the inhibition of endogenous hedgehog by anti-Shh antibody deteriorated cardiac function and induced enlargement of infarct area in the post-MI hearts (32). The discrepancy may come from the different cells of Shh inhibition. Secretion of Shh from other cells including fibroblasts was not inhibited in the cardiomyocyte-specific Shh-deleted mice (Shh-MerCre mice). In neural stem cells, Shh expression is induced via the Notch receptor-mediated activation of cytoplasmic signaling molecules, including Akt, STAT3, and mammalian target of rapamycin (33). Furthermore, it has been also reported that *Shh* is a target gene of NF- κ B in mice (34). EPO is known to activate several signaling pathways, including Akt, STAT, and NF- κ B in various tissues (19, 35). Further studies are needed to clarify the signaling cascade by which EPO upregulates Shh expression in cardiomyocytes.

We previously demonstrated that angiogenesis promotes cardiac hypertrophy in mice during the early phase of pressure overload (30). We do not know why EPO did not induce cardiomyocyte hypertrophy in this study, but there is a possibility that MI itself induces cardiac and cardiomyocyte hypertrophy via increased wall stress, and EPO-induced reduction of infarct size might reduce the wall stress, resulting in prevention of cardiac and cardiomyocyte hypertrophy even with enhanced angiogenesis.

In conclusion, EPO prevented LV remodeling after MI through Shh. We have reported that G-CSF inhibits cardiomyocyte apoptosis by activating the JAK2/STAT3 pathway in cardio-

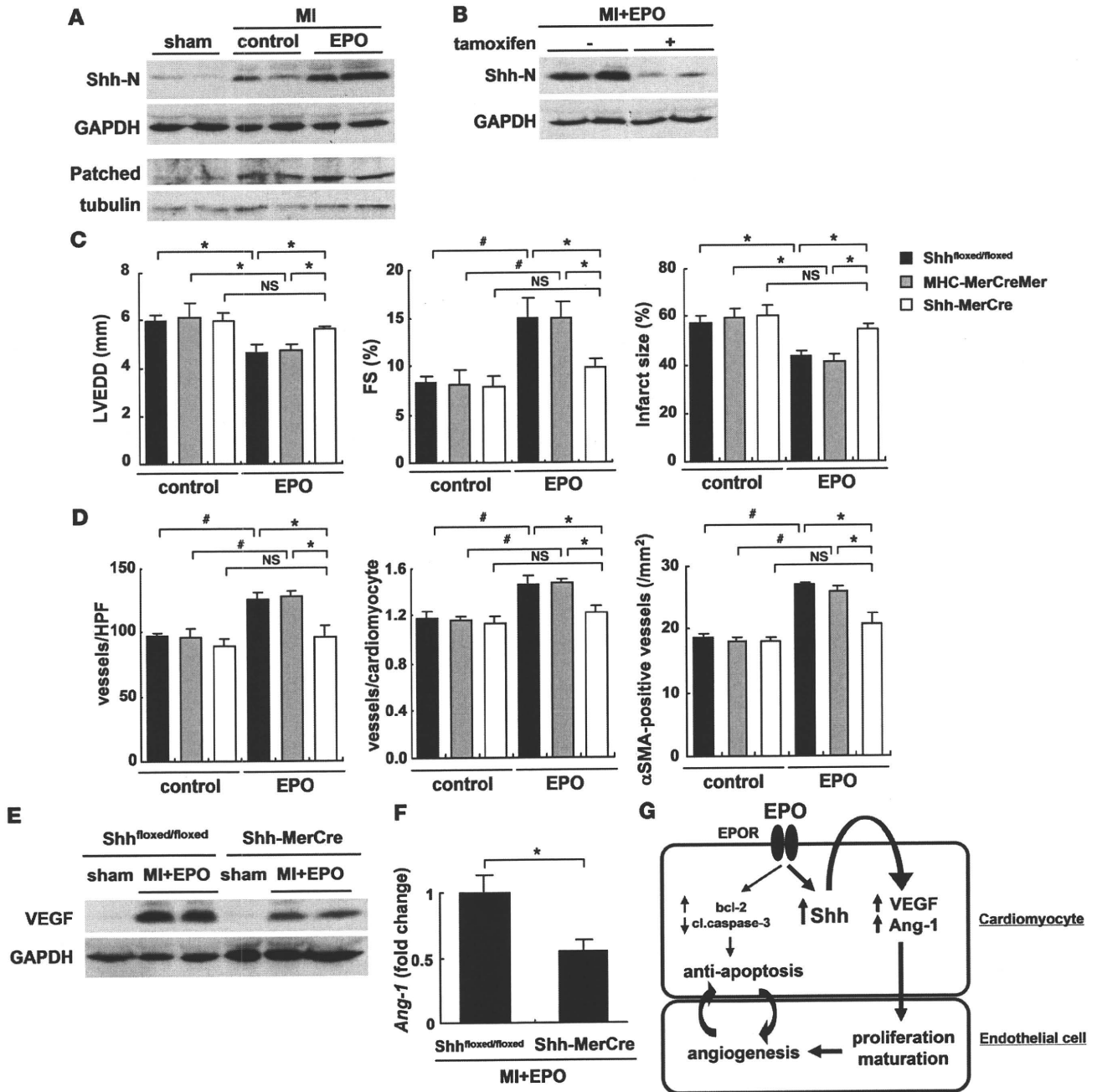


Figure 9

Cardiomyocyte-specific Shh deletion abolishes EPO-induced cardioprotection. (A) Activation of Shh signaling after MI and EPO treatment. Hearts were treated with EPO or saline (control) and harvested 4 days (for Shh-N) or 7 days (for Patched) after MI ($n = 4$ for each). (B) Western blotting of Shh-N in the infarcted hearts from Shh-MerCre mice treated with or without tamoxifen. Mice were subjected to MI, treated with EPO, and sacrificed 4 days after MI ($n = 4$ for each condition). We measured LVEDD, FS, infarct size (C), the number of vessels, the ratio of vessels to cardiomyocyte, and the number of α -SMA-positive vessels (D) 14 days after MI ($n = 8-14$). * $P < 0.05$; # $P < 0.01$. (E and F) Western blotting of VEGF and qRT-PCR analysis of *Ang-1* mRNA in the heart 7 days after MI. All mice were treated with EPO ($n = 5$). * $P < 0.05$. (G) Proposed mechanism underlying the cardioprotective effects of EPO during MI. The mechanisms denoted by the thicker lines are thought to be particularly important.

myocytes, leading to reduced LV remodeling (5). EPO prevented cardiomyocyte apoptosis and protected the heart via the JAK2/STAT3-independent mechanisms, presenting the possibility that administration of the 2 cytokines synergistically protects the heart after MI.

Methods

Animals. All experimental procedures were performed according to the guidelines established by Chiba University for experiments in animals, and all protocols were approved by our institutional review board. Male (C57BL/6 background, 10- to 12-week-old) mice were used in this study.



Shh^{flxed/flxed} mice were purchased from Jackson Laboratory. We injected each mouse with 8 mg/kg of tamoxifen (Sigma-Aldrich) for 12 consecutive days and produced MI at 7 days after tamoxifen treatment. Because EPOR-null mice are embryonic lethal due to severe anemia, we prepared RES mice expressing EPOR exclusively in the hematopoietic lineage, which were established as described previously (15). EPOR expression is limited to the erythroid lineage cells in the RES mice. The RES mice develop normally and are fertile. GFP transgenic mice were purchased from SLC. Generation and genotyping of dnSTAT3-Tg mice have been previously described (36). Age- and sex-matched WT mice (C57BL/6; SLC) were used as controls. RES mice were provided by M. Yamamoto (Tohoku University School of Medicine, Miyagi, Japan).

Induction of MI and treatment. Mice were anesthetized by intraperitoneal injection of pentobarbital (50 mg/kg) and artificially ventilated with a respirator. Mice were subjected to ligation of the left anterior descending artery or to sham operation as described previously (4). Sham operation was performed by cutting pericardium. EPO (Chugai Pharmaceutical) or the same volume of saline was administered subcutaneously.

Echocardiography. Transthoracic echocardiography was performed with a VisualSonics (Vevo 660; VisualSonics Inc.) equipped with a 25-MHz imaging transducer. Mice were kept awake without anesthesia during the echocardiographic examination to minimize data deviation, and heart rate was approximately 550–650 bpm in all mice.

Histology. Hearts fixed in 10% formalin were embedded in paraffin and sectioned at 4- μ m thickness for Masson trichrome staining. Tissue hypoxia was evaluated using the Hypoxyprobe (Chemicon) according to the manufacturer's instructions. Fixed frozen sections of the heart samples were immunohistochemically stained by using primary antibodies to PECAM (PharMingen), dystrophin (Novocastra Laboratories), α -SMA (DAKO), and Mac3 (BD Biosciences). The ischemic area that indicates infarct and border area was measured. For measurement of the cross-sectional area of cardiomyocytes, 50 randomly selected cardiomyocytes in a LV cross-section were measured by tracing dystrophin immunostaining. These measurements were performed with NIH ImageJ software. The samples were stained with Hoechst 33258 (1 μ g/ml) or TO-PRO-3 (Molecular Probes Inc.). Immunofluorescence was visualized by laser confocal microscopy (Radiance 2000; Bio-Rad Laboratories).

Bone marrow transplantation. Bone marrow cells were isolated from 8-week-old transgenic mice systemically expressing GFP or WT mice. Bone marrow cells (5×10^7 cells) suspended in 100 μ l of PBS containing 3% FBS were injected intravenously into irradiated WT mice or RES mice. A flow cytometric analysis revealed that more 97% of bone marrow cells were derived from donor cells at 6 weeks after bone marrow transplantation.

Flow cytometry. Circulating EPCs derived from bone marrow were detected by flow cytometry using CD34/Flk-1 double labeling. Mice subjected to MI or sham operation were treated with EPO or saline for 3 days subsequent to the operation. Then the mice were sacrificed to collect peripheral blood. The nucleated cells were incubated with FITC-conjugated anti-CD34 monoclonal antibody and PE-conjugated anti-Flk-1 antibody (VEGFR2/KDR; BD Biosciences) for 60 minutes on ice and washed with PBS supplemented with 3% FBS. The labeled nucleated cells were analyzed by the EPICS ALTRA flow cytometer using EXPO32 software (Beckman Coulter).

Western blot analysis. Western blot analysis was performed as described previously (30). Briefly, the infarcted hearts were separated into 2 parts consisting of the ischemic and viable regions. Proteins extracted from the ischemic regions of the infarcted hearts of mice were subjected to SDS-PAGE and then transferred onto polyvinylidene difluoride membranes (GE Healthcare). The membranes were probed using a primary antibody against, Shh-N (SE1; Developmental Studies Hybridoma Bank), VEGF, Patched, GAPDH (Santa Cruz Biotechnology Inc.), Ang-1 (Rockland), and α -tubulin (Sigma-Aldrich). For in vitro study, primary antibodies against Shh, Akt, Bcl-2

(Santa Cruz Biotechnology Inc.), VEGF for rat (R&D systems), phospho-Akt, phospho-ERK, cleaved caspase-3 (Cell Signaling), ERK (Invitrogen), and actin (Sigma-Aldrich) were used. The ECL-plus system (GE healthcare) was used for detection. Coomassie Brilliant Blue (Wako Pure Chemical Industries) was used for staining total protein blot with culture medium supernatant of cardiomyocytes.

In vivo gene transfer. Soluble Flt-1 is known to bind to VEGF, thereby acting on as an inhibitor for VEGF (37). We injected an adenoviral vector encoding the murine soluble *Flt-1* gene (10^9 pfu; Invitrogen) into thigh muscles of mice at 4 days before MI and 3 days after MI. Adenoviral vector encoding LacZ (10^9 PFU) was used as control.

Cell culture. Cardiomyocytes prepared from ventricles of 1-day-old Wistar rats were plated onto 35-mm plastic culture dishes at a concentration of 1×10^5 cells/cm² and cultured in DMEM supplemented with 10% FBS at 37°C in a mixture of 95% air and 5% CO₂. The culture medium was changed to serum-free DMEM 24 hours before stimulation. rmShh peptide was purchased from R&D Systems. The plasmid of a truncated form of human EPOR was from Y. Nakamura (RIKEN BioResource Center, Tsukuba, Ibaraki, Japan) (38). Adenoviral vector of truncated EPOR was created using AdEasy Vector System (Qbiogene). Adenoviral vector of dnSTAT3 was a gift from K. Yamauchi-Takahara (Osaka University, Osaka, Japan) (36). siRNA targeting VEGF, Shh, and negative control RNA (Invitrogen) were introduced into rat cardiomyocytes by using Lipofectamine RNAiMAX (Invitrogen) according to the manufacturer's instructions. For immunocytochemical staining, cardiomyocytes and cardiac fibroblasts were cocultured with or without EPO for 48 hours, fixed in 4% paraformaldehyde, and stained with primary antibodies to Shh (Santa Cruz Biotechnology Inc.), α -sarcomeric actinin (Sigma-Aldrich), and vimentin (Progen).

qRT-PCR. qRT-PCR analysis was performed as described previously (39). Total RNA was extracted from sample using the RNeasy kit (QIAGEN). We used 2.5 μ g of total RNA to generate cDNA using the Super Script VILO cDNA synthesis kit (Invitrogen). qRT-PCR was carried out on a LightCycler system (Roche) using probes from Universal Probe Library (Roche) and the TaqMan Master Mix (Roche). Sequence of primers and the respective Universal Probe Library probes were as follows: *Ang-1*: forward GGAAGATGGAAGCCTGGAT, reverse ACCAGAGGGATCCCCAAAC, probe #12; *Gapdh*: forward TGTCGGTCGTGGATCTGAC, reverse CCTGCTTACCACCTTCTTG, probe #80, each for mouse; *Shh*: forward GAATCCAAAGCTCGCATCC, reverse CAGGTGCACTGTGGCTGAT, probe #38; *Ang-1*: forward GGAAGCCTAGATTTCAGAGG, reverse ACCAGAGGGATCCCCAAAC, probe #12; *Ptch-1*: forward CAAAGCTGACTACATGCCAGA, reverse GCGTACTCTATGGGCTCTGC, probe #64; *Gli-1*: forward GGAAGAGAGCAGACTGACTGTG, reverse GGGGAGTG-GTCACTGCTG, probe #1; and *Gapdh*: forward AATGTATCCGTTGTG-GATCTGA, reverse GCTTACCACCTTCTTGATGT, probe #80, each for rat. Relative expression of target genes was calculated with the comparative CT method. Each sample was run in duplicate, and the results were systematically normalized using *Gapdh*.

Apoptosis analysis. Frozen sections of the heart samples and cultured cardiomyocytes fixed by 4% paraformaldehyde were subjected to TUNEL staining using a commercially available kit (In Situ Apoptosis Detection Kit; Takara Biomedicals) as directed by manufacturer. Annexin V-Cy3 Apoptosis Detection Kit (BioVision) was used to detect apoptotic cardiomyocytes according to the manufacturer's instructions. Cultured cardiomyocytes were serum starved in DMEM with 0.5% FBS and treated with EPO (10 U/ml) or normal saline for 8 hours prior to beginning H₂O₂ (100 μ M) treatment. Cyclopamine (40–42) (5 μ M), LY294002 (5 μ M), and PD98059 (10 μ M; Calbiochem) were administered 15 minutes before EPO treatment.



research article

DNA synthesis assay. DNA synthesis was measured by performing a BrdU incorporation assay with a commercially available kit (Roche) as directed by the manufacturer. Cardiomyocyte-conditioned medium was collected as previously described (43). Briefly, cultured cardiomyocytes were starved in DMEM without FBS and were pretreated with EPO (10 U/ml) or saline for 48 hours, and then the medium was collected and transferred to HUVECs. HUVECs were plated in 96-well plates at a density of 5×10^4 cells/well in endothelial cell basal medium-2 with EGM-2 Bullet Kit (Cambrex) for 8 hours and then switched to cardiomyocyte-conditioned medium for 12 hours. BrdU was added to the medium, and BrdU incorporation was detected by ELISA using anti-BrdU antibody. VEGF receptor antagonist CBO-P11 (44, 45) (12 μ M; Calbiochem) and anti-Ang-1 antibody (1 μ g/ml; Chemicon) were used for the inhibition studies.

Tube formation assay. Matrigel (growth factor reduced, 100 μ l; BD Biosciences) was added to each well of a 48-well plate and allowed to polymerize at 37°C for 1 hour. HUVECs (1×10^4) were seeded onto Matrigel in endothelial cell basal medium-2 with EGM-2 Bullet Kit and cultured for 1 hour and then switched to cardiomyocyte-conditioned medium described above. After 8 hours, tube length was quantified using an angiogenesis image analyzer (Kurabo).

Isolated heart perfusion system. Isolated heart perfusion system was used to measure coronary flow as previously described (46). In brief, mouse hearts were excised rapidly and mounted on a Langendorff perfusion system. All isolated hearts were stabilized by perfusion of Krebs-Henseleit buffer, and perfusion pressure was adjusted to 60 mmHg. The heart was paced at 400 bpm. After an adjustment period, the coronary effluent was collected and the coronary flow was calculated. After baseline measure-

ments, sodium nitroprusside (10^{-4} M, Sigma-Aldrich) was infused into the perfusate, and coronary flow was measured.

Statistics. All data are shown as mean \pm SEM. Multiple group comparison was performed by 1-way ANOVA followed by Bonferroni's procedure for comparison of means. Comparison between 2 groups was analyzed by the 2-tailed Student's *t* test. Values of *P* < 0.05 were considered statistically significant.

Acknowledgments

The authors thank M. Yamamoto (Tohoku University School of Medicine, Miyagi, Japan) for generously providing RES mice. The authors thank Y. Ohtsuki, M. Ikeda, I. Sakamoto, A. Furuyama, M. Kikuchi, and H. Maruyama for their excellent technical assistance. This work was supported by a Grant-in-Aid for Scientific Research from the Ministry of Education, Science, Sports, and Culture, and Health and Labor Sciences research grants (to I. Komuro) and a Grant-in-Aid for Scientific Research from the Ministry of Education, Culture, Sports, Science and Technology of Japan and grants from the Terumo Life Science Foundation (to H. Takano).

Received for publication May 18, 2009, and accepted in revised form March 24, 2010.

Address correspondence to: Issei Komuro, Department of Cardiovascular Science and Medicine, Chiba University Graduate School of Medicine, 1-8-1 Inohana, Chuo-ku, Chiba 260-8670, Japan. Phone: 81.43.226.2097; Fax: 81.43.226.2557; E-mail: komuro-tky@umin.ac.jp.

- Jessup M, Brozena S. Heart failure. *N Engl J Med*. 2003;348(20):2007-2018.
- Rosamond W, et al. Heart disease and stroke statistics--2008 update: a report from the American Heart Association Statistics Committee and Stroke Statistics Subcommittee. *Circulation*. 2008;117(4):e25-146.
- Moon C, et al. Erythropoietin reduces myocardial infarction and left ventricular functional decline after coronary artery ligation in rats. *Proc Natl Acad Sci U S A*. 2003;100(20):11612-11617.
- Ohtsuka M, et al. Cytokine therapy prevents left ventricular remodeling and dysfunction after myocardial infarction through neovascularization. *FASEB J*. 2004;18(7):851-853.
- Harada M, et al. G-CSF prevents cardiac remodeling after myocardial infarction by activating the Jak-Stat pathway in cardiomyocytes. *Nat Med*. 2005;11(3):305-311.
- Silverberg DS, et al. The effect of correction of mild anemia in severe, resistant congestive heart failure using subcutaneous erythropoietin and intravenous iron: a randomized controlled study. *J Am Coll Cardiol*. 2001;37(7):1775-1780.
- Ponikowski P, et al. Effect of darbepoetin alfa on exercise tolerance in anemic patients with symptomatic chronic heart failure: a randomized, double-blind, placebo-controlled trial. *J Am Coll Cardiol*. 2007;49(7):753-762.
- Felker GM, Adams KF Jr, Gattis WA, O'Connor CM. Anemia as a risk factor and therapeutic target in heart failure. *J Am Coll Cardiol*. 2004;44(5):959-966.
- Bahlmann FH, et al. Erythropoietin regulates endothelial progenitor cells. *Blood*. 2004;103(3):921-926.
- Parsa C, et al. A novel protective effect of erythropoietin in the infarcted heart. *J Clin Invest*. 2003;112(7):999-1007.
- Wright GL, Hanlon P, Amin K, Steenbergen C, Murphy E, Arcasoy MO. Erythropoietin receptor expression in adult rat cardiomyocytes is associated with an acute cardioprotective effect for recombinant erythropoietin during ischemia-reperfusion injury. *FASEB J*. 2004;18(9):1031-1033.
- Brines M, Cerami A. Emerging biological roles for erythropoietin in the nervous system. *Nat Rev Neurosci*. 2005;6(6):484-494.
- Tada H, et al. Endogenous erythropoietin system in non-hematopoietic lineage cells plays a protective role in myocardial ischemia/reperfusion. *Cardiovasc Res*. 2006;71(3):466-477.
- Asaumi Y, et al. Protective role of endogenous erythropoietin system in nonhematopoietic cells against pressure overload-induced left ventricular dysfunction in mice. *Circulation*. 2007;115(15):2022-2032.
- Suzuki N, et al. Erythroid-specific expression of the erythropoietin receptor rescued its null mutant mice from lethality. *Blood*. 2002;100(7):2279-2288.
- Li Y, et al. Reduction of inflammatory cytokine expression and oxidative damage by erythropoietin in chronic heart failure. *Cardiovasc Res*. 2006;71(4):684-694.
- Hirose S, et al. Erythropoietin attenuates the development of experimental autoimmune myocarditis. *Cardiovasc Drugs Ther*. 2007;21(1):17-27.
- Abbate A, Biondi-Zoccai GG, Baldi A. Pathophysiologic role of myocardial apoptosis in post-infarction left ventricular remodeling. *J Cell Physiol*. 2002;193(2):145-153.
- Latini R, Brines M, Fiordaliso F. Do non-hemopoietic effects of erythropoietin play a beneficial role in heart failure? *Heart Fail Rev*. 2008;13(4):415-423.
- Pağes G, Pouyssegur J. Transcriptional regulation of the Vascular Endothelial Growth Factor gene—a concert of activating factors. *Cardiovasc Res*. 2005;65(3):564-573.
- Wang L, et al. The sonic hedgehog pathway mediates carbamylated erythropoietin-enhanced proliferation and differentiation of adult neural progenitor cells. *J Biol Chem*. 2007;282(42):32462-32470.
- Polá R, et al. The morphogen sonic hedgehog is an indirect angiogenic agent upregulating two families of angiogenic growth factors. *Nat Med*. 2001;7(6):706-711.
- Kusano KF, et al. Sonic hedgehog myocardial gene therapy: tissue repair through transient reconstitution of embryonic signaling. *Nat Med*. 2005;11(11):1197-1204.
- Washington Smoak I, et al. Sonic hedgehog is required for cardiac outflow tract and neural crest cell development. *Dev Biol*. 2005;283(2):357-372.
- Lewis PM, et al. Cholesterol modification of sonic hedgehog is required for long-range signaling activity and effective modulation of signaling by Ptc1. *Cell*. 2001;105(5):599-612.
- Sohal DS, et al. Temporally regulated and tissue-specific gene manipulations in the adult and embryonic heart using a tamoxifen-inducible Cre protein. *Circ Res*. 2001;89(1):20-25.
- Suri C, et al. Increased vascularization in mice overexpressing angiotensin-1. *Science*. 1998;282(5388):468-471.
- Asahara T, et al. Tie2 receptor ligands, angiotensin-1 and angiotensin-2, modulate VEGF-induced postnatal neovascularization. *Circ Res*. 1998;83(3):233-240.
- Holash J, Wiegand SJ, Yancopoulos GD. New model of tumor angiogenesis: dynamic balance between vessel regression and growth mediated by angiopoietins and VEGF. *Oncogene*. 1999;18(38):5356-5362.
- Sano M, et al. p53-induced inhibition of Hif-1 causes cardiac dysfunction during pressure overload. *Nature*. 2007;446(7134):444-448.
- Giordano FJ, et al. A cardiac myocyte vascular endothelial growth factor paracrine pathway is required to maintain cardiac function. *Proc Natl Acad Sci U S A*. 2001;98(10):5780-5785.
- Lavine KJ, Kovacs A, Ornitz DM. Hedgehog signaling is critical for maintenance of the adult coronary vasculature in mice. *J Clin Invest*. 2008;118(7):2404-2414.
- Androussellis-Theotokis A, et al. Notch signaling regulates stem cell numbers in vitro and in vivo. *Nature*. 2006;442(7104):823-826.
- Kasperczyk H, Baumann B, Debatin KM, Fulda S. Characterization of sonic hedgehog as a novel



- NF-kappaB target gene that promotes NF-kappaB-mediated apoptosis resistance and tumor growth in vivo. *FASEB J*. 2009;23(1):21-33.
35. Digicaylioglu M, Lipton SA. Erythropoietin-mediated neuroprotection involves cross-talk between Jak2 and NF-kappaB signalling cascades. *Nature*. 2001;412(6847):641-647.
36. Funamoto M, et al. Signal transducer and activator of transcription 3 is required for glycoprotein 130-mediated induction of vascular endothelial growth factor in cardiac myocytes. *J Biol Chem*. 2000;275(14):10561-10566.
37. Kendall RL, Thomas KA. Inhibition of vascular endothelial cell growth factor activity by an endogenously encoded soluble receptor. *Proc Natl Acad Sci U S A*. 1993;90(22):10705-10709.
38. Nakamura Y, Komatsu N, Nakauchi H. A truncated erythropoietin receptor that fails to prevent programmed cell death of erythroid cells. *Science*. 1992;257(5073):1138-1141.
39. Leucht C, Stigloher C, Wizenmann A, Klafke R, Folchert A, Bally-Cuif L. MicroRNA-9 directs late organizer activity of the midbrain-hindbrain boundary. *Nat Neurosci*. 2008;11(6):641-648.
40. Taipale J, et al. Effects of oncogenic mutations in Smoothened and Patched can be reversed by cyclopamine. *Nature*. 2000;406(6799):1005-1009.
41. Berman D, et al. Medulloblastoma growth inhibition by hedgehog pathway blockade. *Science*. 2002;297(5586):1559-1561.
42. Watkins DN, Berman DM, Burkholder SG, Wang B, Beachy PA, Baylin SB. Hedgehog signalling within airway epithelial progenitors and in small-cell lung cancer. *Nature*. 2003;422(6929):313-317.
43. Zhang Y, Pasparakis M, Kollias G, Simons M. Myocyte-dependent regulation of endothelial cell syndecan-4 expression. Role of TNF-alpha. *J Biol Chem*. 1999;274(8):4786-4790.
44. Zilberberg L, et al. Structure and inhibitory effects on angiogenesis and tumor development of a new vascular endothelial growth inhibitor. *J Biol Chem*. 2003;278(37):35564-35573.
45. Heineke J, et al. Cardiomyocyte GATA4 functions as a stress-responsive regulator of angiogenesis in the murine heart. *J Clin Invest*. 2007;117(11):3198-3210.
46. Bendall J, et al. C. Strain-dependent variation in vascular responses to nitric oxide in the isolated murine heart. *J Mol Cell Cardiol*. 2002;34(10):1325-1333.

Increased Akt-mTOR Signaling in Lung Epithelium Is Associated with Respiratory Distress Syndrome in Mice[∇]

Hiroyuki Ikeda,^{1,2} Ichiro Shiojima,^{1,3} Toru Oka,^{1,3} Masashi Yoshida,¹ Koji Maemura,⁴ Kenneth Walsh,⁵ Takashi Igarashi,² and Issei Komuro^{1,3*}

Department of Cardiovascular Science and Medicine, Chiba University Graduate School of Medicine, Chiba, Japan¹; Department of Pediatrics, University of Tokyo Graduate School of Medicine, Tokyo, Japan²; Department of Cardiovascular Medicine, Osaka University Graduate School of Medicine, Suita, Japan³; Department of Cardiovascular Medicine, Nagasaki University Graduate School of Biomedical Sciences, Nagasaki, Japan⁴; and Molecular Cardiology, Whitaker Cardiovascular Institute, Boston University School of Medicine, Boston, Massachusetts⁵

Received 24 June 2010/Returned for modification 31 August 2010/Accepted 17 December 2010

Pregnancy in women with diabetes is associated with a higher risk of perinatal complications. In particular, infants of diabetic mothers frequently suffer from respiratory distress syndrome (RDS), which is a leading cause of death in preterm infants and is considered to be primarily due to hyperinsulinemia in infants in response to maternal hyperglycemia. To elucidate the mechanism of how insulin signaling induces RDS, bronchoalveolar epithelium-specific Akt1 transgenic (TG) mice were generated. Akt1 overexpression in fetal lung epithelium resulted in RDS in preterm infants born by Caesarean section at embryonic day 18.5 (E18.5). The expression levels of hypoxia-inducible factor 2 α (HIF-2 α) and its target vascular endothelial growth factor (VEGF) were downregulated in the lung of Akt1 TG mice. Inhibition of the Akt-mammalian target of rapamycin (mTOR) signaling axis by rapamycin restored the expression of VEGF and improved the lung pathology of Akt1 TG pups. Rapamycin also attenuated the RDS phenotype in wild-type mice delivered preterm at E17.5. In cultured lung epithelial cells, insulin reduced VEGF expression and transcriptional activity of HIF-2 on VEGF promoter in an mTOR-dependent manner. Thus, aberrant activation of the Akt-mTOR pathway in lung epithelium plays a causal role in the pathogenesis of infant RDS, presumably through downregulation of HIF-2-dependent VEGF expression in the lung.

Pregnancy in women with diabetes is associated with a higher risk of perinatal complications. The estimated prevalence rate of gestational diabetes is approximately 4% and is considered to represent 90% of all cases of diabetes diagnosed during pregnancy (2). Moreover, pregnant women with type 2 diabetes are increasing in number in line with the rapid increase in the prevalence of type 2 diabetes in all age groups (9). Infants of diabetic mothers frequently suffer from macrosomia, neonatal hypoglycemia, cardiomegaly, respiratory difficulties, and other congenital anomalies (3, 5, 14, 21), which are considered to be primarily due to hyperinsulinemia in infants in response to maternal hyperglycemia. Respiratory distress syndrome (RDS) is one of the most clinically significant perinatal complications, with high morbidity and mortality (19, 22). RDS is caused by attenuated production of pulmonary surfactant, a mixture of phospholipids and surfactant-associated proteins that covers the alveolar surface and prevents alveolar collapse by reducing the surface tension of the air-water interface (12). Because pulmonary surfactant is specifically produced by type II lung epithelial cells, attenuated production of pulmonary surfactant is considered to be due to impaired differentiation and/or maturation of type II lung epithelial cells (31). Reduced expression of surfactant-associated proteins was observed in fetuses of streptozotocin-induced diabetic rats or in insulin-treated human fetal lung explants (8, 10, 11), suggesting that

hyperactivation of insulin signaling in the lung plays a causal role in the pathogenesis of RDS of infants having a diabetic mother.

Phosphatidylinositol 3-kinase (PI3K) is activated by insulin and is responsible for most of the metabolic actions of insulin. PI3K also controls cell growth, differentiation, survival, and protein synthesis (28). The involvement of the PI3K pathway in RDS was suggested by a previous report showing that bronchoalveolar-specific deletion of *Pten* in mice led to upregulation of the PI3K pathway in the lung and resulted in RDS associated with marked hyperplasia of alveolar epithelial cells, increased numbers of bronchoalveolar stem cells (BASCs), and impaired production of surfactant proteins (SPs) (33). It was also shown that genetic ablation of hypoxia-inducible factor 2 α (HIF-2 α) causes RDS due to downregulation of vascular endothelial growth factor (VEGF) expression in the lung and that intratracheal VEGF administration stimulates maturation of type II lung epithelial cells (4). However, the downstream effectors of PI3K that cause RDS and the mechanistic link between the PI3K pathway and HIF-2-dependent VEGF expression in the lung have been elusive.

Using bronchoalveolar epithelium-specific Akt1 transgenic (TG) mice, we show here that aberrant activation of the Akt-mammalian target of rapamycin (mTOR) pathway in lung epithelium plays a causal role in the pathogenesis of infant RDS. We also provide evidence suggesting that sustained Akt-mTOR activation induces RDS through downregulation of HIF-2-dependent VEGF expression in the lung.

MATERIALS AND METHODS

Animals and DOX administration. SP-C-rtTA TG mice expressing the reverse tetracycline transactivator (rtTA) protein under the control of the human surfactant protein-C promoter (pro-SP-C) on the FVB/N background were de-

* Corresponding author. Mailing address: Department of Cardiovascular Medicine, Osaka University Graduate School of Medicine, 2-2 Yamadaoka, Suita 565-0871, Japan. Phone: 81 6 6879 3631. Fax: 81 6 6879 3639. E-mail: komuro-tky@umin.ac.jp.

[∇] Published ahead of print on 28 December 2010.

scribed previously (23, 29) and were purchased from the Jackson Laboratory. These mice were crossed with Tet-myrAkt1 TG mice (25) harboring a myristoylated Akt1 (myrAkt1) transgene under the control of multimerized *tetO* sequences maintained on a mixed background of FVB/N, C57BL/6J, and 129Sv. For myrAkt1 expression, dams were treated with doxycycline (DOX) in drinking water from embryonic day 0.5 (E0.5) at a final concentration of 0.5 mg/ml (25, 29). Respiratory rate was measured by visual inspection of the movements of thorax and abdomen for 1 min. All animal procedures were performed with the approval of the Institutional Animal Care and Use Committee of Chiba University.

Histological analysis and immunohistochemistry. Lungs were formalin fixed without constant pressure inflation and embedded in paraffin for histological analyses. Serial sections of 4 μ m were stained with hematoxylin and eosin (HE) for morphological analysis, periodic acid-Schiff (PAS) for detection of glycogen-rich cells, and Masson's trichrome (MT) for detection of fibrosis. Aerated lung area and alveolar septal thickness were measured in toluidine blue-stained sections using ImageJ software (4). Aerated lung area was measured in 10 visual fields for each animal. Septal thickness was measured at 10 points in each visual field, and 10 visual fields for each animal were used for the measurement. The size and number of saccules were measured in PAS-stained sections using ImageJ software. The size of 10 saccules was measured in each visual field, and 10 visual fields for each animal were used for the analysis. Saccular number was counted in 10 visual fields for each animal. Immunohistochemistry was performed using an avidin-biotin-horseradish peroxidase detection system with Ni-diaminobenzidine (DAB) (ABC kit; Vector Laboratories) and Nuclear Fast Red as a counterstain. The antibodies used were hemagglutinin (HA), pro-SP-C, Clara cell 10-kDa protein (CC10), aquaporin-5 (AQP5), VEGF (Santa Cruz Biotechnology), and calcitonin gene-related peptide (CGRP; BioMol).

Fluorescence imaging. A BZ-9000 (Keyence) microscope was used for fluorescence imaging. Paraffin-embedded lung sections were incubated with isolectin B4-fluorescein isothiocyanate (FITC) conjugate (Sigma) to detect endothelial cells and with wheat germ agglutinin-tetramethyl rhodamine isothiocyanate (TRITC) conjugate (Sigma) to counterstain the cell membrane. Vascular cell counts with three replications were performed with BZ application software (Keyence), and the median value was used for each sample.

Western blot analysis. Total protein lysate was extracted from lung tissue, and SDS-PAGE was performed as described previously (26). The antibodies used were HA, total Akt1, total S6 kinase (S6K), SP-A, pro-SP-C, AQP5, CC10, VEGF, glyceraldehyde-3-phosphate dehydrogenase (GAPDH; Santa Cruz Biotechnology), phospho-Akt (Ser473), phospho-S6K1 (Thr389), phospho-S6 (Ser235/236), total S6, phospho-glycogen synthase kinase 3 β (phospho-GSK3 β) (Ser9), phospho-FOXO3a (318/321), total FOXO3a (Cell Signaling Technology), SP-B, SP-D (Chemicon/Millipore), and HIF-2 α (Novus Biologicals). Densitometric analysis was performed using ImageJ.

Mouse model of preterm infants. Pups were collected by Caesarean section at E18.5 for Akt1 TG mice and at E17.5 for wild-type ICR mice (4, 20). The umbilical cord was cut, amniotic fluid and membranes were removed from the mouth and nose, and body temperature was kept at 37°C.

Administration of rapamycin. Rapamycin (LC Laboratories) was prepared in the solvent containing 0.2% sodium carboxymethylcellulose and 0.25% polysorbate-80 in water (24, 25). Rapamycin (1 mg/kg of body weight/day) or vehicle was administered subcutaneously to dams.

Reporter gene assays. Luciferase assays were performed essentially as previously described (18). The plasmids used were VEGF reporter plasmid (pGL2hVEGF) and the expression vectors for HIF-1 α (phHIF-1 α), HIF-2 α (phEP-1), and ARNT (phARNT). A549 cells were transfected with the plasmids indicated in the Fig. 8 legend and treated with 250 μ M CoCl₂ to mimic hypoxic condition.

Statistical analysis. Data are expressed as means \pm standard errors of the means (SEM). Statistical significance between two groups was determined with a Student's *t* test or χ^2 test. Probability values of <0.05 were considered to be statistically significant.

RESULTS

Generation of bronchoalveolar epithelium-specific Akt1 TG mice. Two lines of TG mice (Tet-myrAkt1 and SP-C-rtTA) were used to generate bronchoalveolar epithelium-specific Akt1 TG mice (Fig. 1A). The Tet-myrAkt1 TG line harbors an active form of the Akt1 transgene (myrAkt1) under the control of multimerized tetracycline operator (*tetO*) sequences (25), and the SP-C-rtTA TG line expresses the reverse tetracycline

transactivator (rtTA) in respiratory epithelial cells driven by human surfactant protein-C (SP-C) promoter (23, 29). DOX enables rtTA binding to *tetO* sequences by inducing its conformational change. Therefore, DOX treatment of double-TG (DTG) mice harboring both transgenes induces transcription of the myrAkt1 gene in lung epithelial cells (Fig. 1A). Mating of SP-C-rtTA mice with Tet-myrAkt1 mice resulted in the generation of mice with four different genotypes (wild type, Tet-myrAkt1 single TG, SP-C-rtTA single TG, and DTG) at the expected frequencies. Western blot analysis of lung lysates harvested at postnatal day 0 (P0) revealed that the transgene product detected by anti-HA blotting was observed in the lung of DTG mice treated with DOX (Fig. 1B). The induced expression of myrAkt1 was associated with a marked increase in phosphorylation levels of several downstream effectors such as S6K1, S6, and glycogen synthase kinase-3 (GSK3), but not FOXO3 (Fig. 1B). Because it was reported that treatment of SP-C-rtTA mice with DOX may exert toxic effects on alveolar epithelial cells (20), the phenotype of DOX-treated SP-C-rtTA single-TG mice was carefully compared with littermates of other genotypes (wild type, Tet-myrAkt1 single TG, and DTG). However, although there was an obvious lung phenotype in DTG mice (described in detail below), no apparent abnormality was observed in mice with other genotypes under our experimental conditions (Fig. 1C and D). We therefore used DOX-treated single-TG littermates as controls in this study.

Akt activation in lung epithelial cells *in utero* results in transient tachypnea associated with delayed maturation of the lung. Activation of Akt signaling in the lung was achieved by DOX treatment of dams starting at embryonic day 0.5 (E0.5). When analyzed at P0, DTG pups were viable and exhibited no cyanosis or growth retardation (Fig. 2A). Postnatal growth of DTG animals was also comparable to that of control mice. However, DTG mice at P0 exhibited significant tachypnea (Fig. 2B) and various histological abnormalities such as markedly reduced aerated space, increased atelectasis, bronchiolar hyperplasia, impaired thinning of the alveolar septa, and abundant PAS-positive glycogen stores (Fig. 2C to E). Since PAS-positive glycogen is normally converted to surfactant phospholipids in mature epithelial cells, these observations suggest that the differentiation of lung epithelial cells is impaired by aberrant activation of Akt signaling. Of note, these histological findings were improved spontaneously at P2 (Fig. 2C to E). Although mild elastic fiber deposition was observed at P2, no such pathology was evident at the age of 12 weeks (data not shown). Thus, Akt activation in lung epithelium induces transient respiratory difficulties associated with lung maturational defects, which improves spontaneously after birth.

Akt activation in lung epithelial cells *in utero* results in increased numbers of CC10/SP-C double-positive cells and defective maturation of lung epithelial cells. In order to further assess the extent of epithelial differentiation, we performed Western blot analysis of surfactant proteins (SP-A to SP-D) and immunohistochemistry of marker proteins: SP-C for type II alveolar epithelial cells, Clara cell 10-kDa protein (CC10) for Clara cells, aquaporin-5 (AQP5) for type I alveolar epithelial cells, and calcitonin gene-related peptide (CGRP) for neuroendocrine cells. Western blot analysis of surfactant proteins revealed downregulation of SP-B and upregulation of

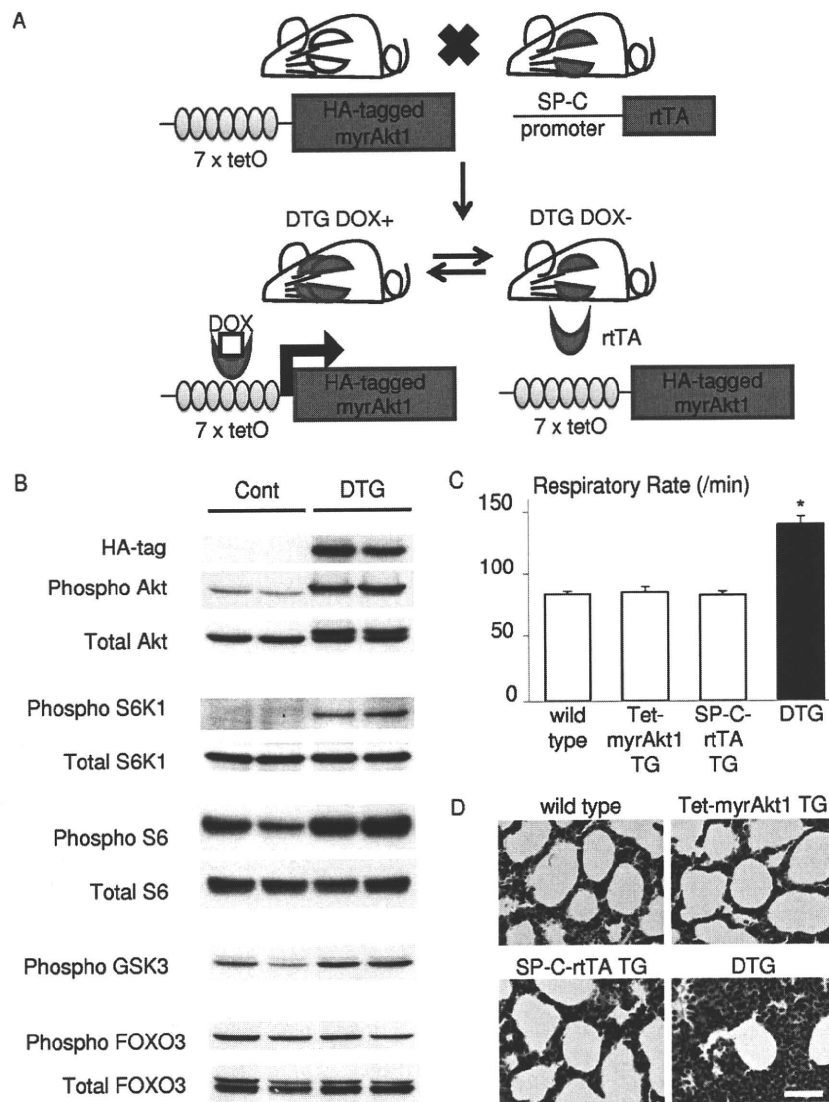


FIG. 1. Generation of bronchoalveolar epithelium-specific Akt1 TG mice. (A) Schematic illustration of binary TG system. (B) Western blot analysis of the whole-lung lysate from control and DTG mice at P0. (C) Respiratory rate at P0. DOX-treated SP-C-rTA TG mice do not show respiratory distress. *, $P < 0.05$ versus DOX-treated wild-type, Tet-myAkt1 TG mice, and SP-C-rTA TG mice ($n = 7, 5, 6,$ and 6 mice, respectively, from 3 dams). All animals were treated with DOX in the drinking water. (D) HE staining of the lung sections. Scale bar, $50 \mu\text{m}$.

SP-D, whereas the expression levels of SP-A and SP-C were not altered (Fig. 3A). Western blot analysis and immunohistochemistry also revealed increased expression of CC10 and reduced expression of AQP5 in the lung of DTG mice (Fig. 3A and B). CGRP expression was not altered between control and DTG mice (date not shown). Previous studies characterized CC10/SP-C double-positive cells as BASCs that reside at the bronchoalveolar duct junction and differentiate to both Clara cells and type II alveolar epithelial cells; the latter further differentiate to type I alveolar epithelial cells (15). Double immunostaining revealed that CC10/SP-C double-positive cells were increased in number in the lung of DTG mice (Fig. 3C and D). Collectively, these findings suggest that aberrant activation of Akt signaling in lung epithelial cells results in increased numbers of CC10/SP-C double-positive cells and impaired differentiation of alveolar epithelial cells.

Akt activation in lung epithelial cells *in utero* results in RDS in preterm infants. Since RDS is more frequent in preterm infants than in full-term infants, we examined preterm infants born by Caesarean section at E18.5. DTG mice born at E18.5 showed cyanosis (Fig. 4A) associated with an irregular respiratory pattern, and all DTG mice died by 2 h after birth (Fig. 4B). The airway spaces of DTG lungs were filled with amorphous, proteinaceous material that was not observed in control lungs (Fig. 4C). PAS staining revealed that the size and the density of saccules in DTG lung were smaller and higher than those of controls, respectively (Fig. 4D to F). Western blot analysis of surfactant proteins revealed downregulation of SP-B, whereas the expression levels of SP-A, -C, and -D were not altered (Fig. 4G). Immunohistochemistry also revealed expansion of CC10/SP-C double-positive cells in the lung of DTG mice (Fig. 4H to J). AQP5 expression was barely detect-